TECHNISCHE UNIVERSITÄT WIEN

DIPLOMARBEIT

SO_3 Contamination in Gas Turbines

im Rahmen des Studiums

Technische Chemie

eingereicht von

Parul Bishnoi BSc

Matrikelnummer 01126195

ausgeführt am Imperial College London (Department of Materials)
in Verbindung mit Solar Turbines Inc

Betreuung

Ao.Univ.Prof. Dipl.-Ing. Dr.techn. **Paul Linhardt,** Technische Universität Wien

Dr. **Stella Pedrazzini,** Imperial College London

Dr. **Ifan E.L. Stephens,** Imperial College London

Dr. **Noel Glaenzer,** Solar Turbines Inc.

Wien, 10. Juni 2021

Ort, Datum | Unterschrift Verfasser | Unterschrift Betreuer

Collaboration and supervision

This work was carried out as part of an Erasmus$^+$ internship and supervised by Prof. Paul Linhardt. The supervisors from Imperial College London were Dr. Stella Pedrazzini and Dr. Ifan E. L. Stephens. The work was done in cooperation with Solar Turbines Inc. (Dr. Noel Glaenzer). The laboratory experiments were carried out at the Vienna University of Technology in the research group of Dr. Helmut Riedl-Tragenreif together with Dipl. Ing. Oliver E. Hudak.

Acknowledgements

Thanks are due to Prof. Paul Linhardt, who always had an open ear for my questions and a quick approach to solving them. The success of this thesis would have not been possible without his supervision. Moreover, I want to express my gratitude to Dr. Stella Pedrazzini for not only the supervision of this thesis, but also for providing me with a vibrant and supportive environment to work on. I would also like to thank each and every member of the research group who have given me a warm welcome during the difficult time of the pandemic. Moreover, I wish to thank Dr. Ifan E. L. Stephens and my industrial supervisor Dr. Noel Glaenzer (Solar Turbines Inc.) for the numerous interesting conversations and advice. I would also like to pay my special regards to Dr. Helmut Riedl-Tragenreif who let me work on short-notice in his research group Applied Surface Technology and to Dipl. Ing. Oliver E. Hudak, who supported and worked with me during the laboratory work. Last but not least, I would like to thank my husband Tim, my parents Sunita and Brahma, my sister Nikita, my parents-in-law Andrea and Christian and my brothers-in-law Alexander and Klaus for always supporting me in every possible way and therefore, helping me to achieve my goals.

Abstract

To operate a gas turbine, fuel gas, often containing a significant amount of H_2S up to 1%, is ignited in the combustion chamber. As soon as sulfur is present in fossil fuels, SO_2 is formed during combustion and further oxidation to SO_3 cannot be avoided. It is known that SO_3 can lead to rapid degradation in the nickel superalloy turbine blades of a gas turbine. Currently there are no reliable methods to predict the amount of SO_3 formed under different conditions.

In the framework of this thesis the SO_2-SO_3 equilibrium was modelled to simulate the influence of different conditions on the formation of SO_3 using the computer program "Chemical Equilibrium with Application". Thermodynamic calculations indicate that CO_2 has no influence on the formation of SO_3 and the higher the SO_2 concentration, the higher the SO_3 concentration. According to the calculations the formation of SO_3 is favoured at low temperatures. The influence of temperature on the formation of SO_3 was further investigated with the help of chemical kinetics software Cantera used with Python. The results confirm that the SO_2:SO_3-ratio decreases at low temperatures. The thermokinetic simulation by Cantera indicates that SO_2 concentration decreases much faster at temperatures above the equilibrium temperature.

The measurement of SO_3 proves to be very difficult since SO_3 is a highly reactive gas and not easily differentiated from the parent molecule SO_2. The isopropanol absorption method was tested to measure the SO_3 content and as a result the experiments clearly show that the presence of the catalyst Al_2O_3 favours the formation of SO_3. A successfully functioning SO_3 measurement technique could be used to measure the influence of different parameters on the formation of SO_3. From this, one could verify the model and, depending on the environment, design the engine in such a way that corrosion is as low as possible.

Kurzfassung

Für den Betrieb einer Gasturbine wird Brenngas in der Brennkammer gezündet, welches oft einen erheblichen Anteil an H_2S (bis zu 1 %) enthält. Sobald Schwefel in fossilen Brennstoffen vorhanden ist, entsteht bei der Verbrennung SO_2 und die weitere Oxidation zu SO_3 ist unvermeidbar. Es ist bekannt, dass SO_3 zu einer schnellen Degradation der Turbinenschaufeln einer Gasturbine, welche aus Nickelsuperlegierung besteht, führen kann. Derzeit gibt es keine zuverlässigen Methoden zur Vorhersage der Menge an SO_3, welches unter verschiedenen Bedingungen gebildet wird.

Im Rahmen dieser Arbeit wurde das SO_2-SO_3-Gleichgewicht modelliert, um den Einfluss verschiedener Bedingungen auf die Bildung des SO_3 mit Hilfe des Computerprogramms "Chemical Equilibrium with Application" zu simulieren. Die thermodynamischen Berechnungen zeigen, dass CO_2 keinen Einfluss auf die Bildung von SO_3 hat und je höher die SO_2-Konzentration ist, desto höher ist auch die SO_3-Konzentration. Gemäß den Berechnungen wird die Bildung von SO_3 bei niedrigen Temperaturen begünstigt. Der Einfluss der Temperatur auf die Bildung von SO_3 wurde mit Hilfe der Thermokinetiksoftware Cantera, die mit Python verwendet wird, weiter untersucht. Die Ergebnisse bestätigen, dass das SO_2:SO_3-Verhältnis bei niedrigen Temperaturen abnimmt. Die thermokinetische Simulation mit Cantera zeigt, dass die SO_2-Konzentration bei Temperaturen oberhalb der Gleichgewichtstemperatur rascher abnimmt.

Die Messung von SO_3 erweist sich als sehr schwierig, da SO_3 ein hochreaktives Gas ist und sich nur schwer vom Grundmolekül SO_2 unterscheiden lässt. Zur Messung des SO_3-Gehalts wurde die Isopropanol-Absorptionsmethode eingesetzt. Die Ergebnisse dieses Experiments zeigen eindeutig, dass die Anwesenheit des Katalysators Al_2O_3 die Bildung von SO_3 begünstigt. Mit einer erfolgreich funktionierenden SO_3-Messtechnik könnte man den Einfluss verschiedener Parameter auf die Bildung von SO_3 messen und daraus ein Modell erstellen.

Contents

Chapter 1

Background

1.1 Gas Turbines

Before dealing specifically with the different SO_3 measurement techniques and the impact of different environmental conditions on the formation of SO_2 and SO_3, it is only appropriate to briefly describe how gas turbines work, what material the turbine blades are made of, and the problem with sulfidation in general.

A gas turbine is a constant pressure combustion engine, that means a machine in which a fuel is burned to generate power. Gas turbines are used in combined cycle power plants where they generate electrical energy. The operating principle is based on the Brayton cycle [1] and therefore, consists of two isentropic and two isobaric processes.

As can be seen in figure 1.1 a gas turbine is composed of a compressor, a combustor and a turbine [1]. The compressor draws in air in ambient conditions from the environment, compresses it and finally feeds it into the combustion chamber. There it is mixed with natural gas or liquid fuel such as diesel or kerosene, then ignited and continuously burned at almost constant pressure. The combustion process is a chemical oxidation reaction involving fuel and air. To ensure complete combustion, the gases must be present in a stoichiometric ratio [2]. In reality, Solar Turbines Inc. uses a mixture slightly below stoichiometric ratio (lean burn) to prevent the formation of contaminants e.g. NO_x. Due to the exothermic reaction of the oxygen-hydrocarbon mixture, the temperature rises to 1400°C [2]. The heated air exits the combustor and enters the turbine inlet at high speed. An expansion takes place in the turbine and the enthalpy contained in the gas is converted into mechanical

energy.

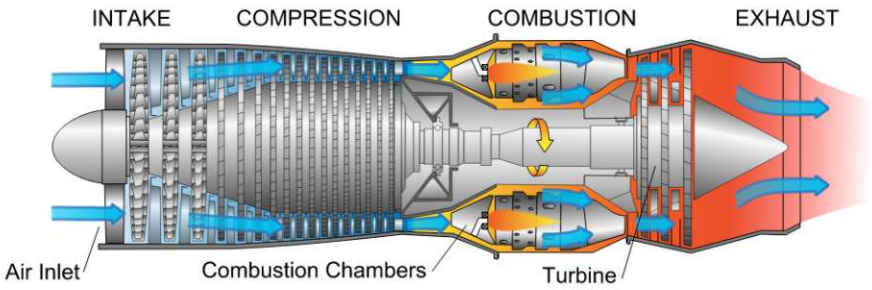

Figure 1.1: Main parts of a gas turbine [3].

1.2 Nickel-based superalloys

To enable higher engine efficiencies, a higher temperature difference across the power turbine is required, but the turbine inlet temperature is limited by the maximum permissible material temperature.

High-temperature materials include all materials that can be used permanently approximately above 500°C [4]. Nickel superalloys are an example of high-temperature materials and are well known for their creep and fatigue strength. They can be operated above 1650°C and thus above their melting point (melting point of Ni = 1455°C). The operating temperatures can exceed the melting point of the high temperature materials. For this reason, the turbine blades are cooled both internally and externally and often have a thermal barrier coating (TBC) i.e. a ceramic coating of e.g. yttria-stabilized zirconia (YSZ) for protection [5]. Since grain boundaries are sites where damage can accumulate, these materials can be enhanced if they are solidified in a preferred direction. The directional solidification of alloys, characterised by a columnar crystal structure, can expand the creep life of the blade and the operating temperature can be increased (figure 1.2) [3]. Nowadays, turbine blades often consist of a single crystal, which is particularly resistant to mechanical stress due to an elimination of grain boundaries [7].

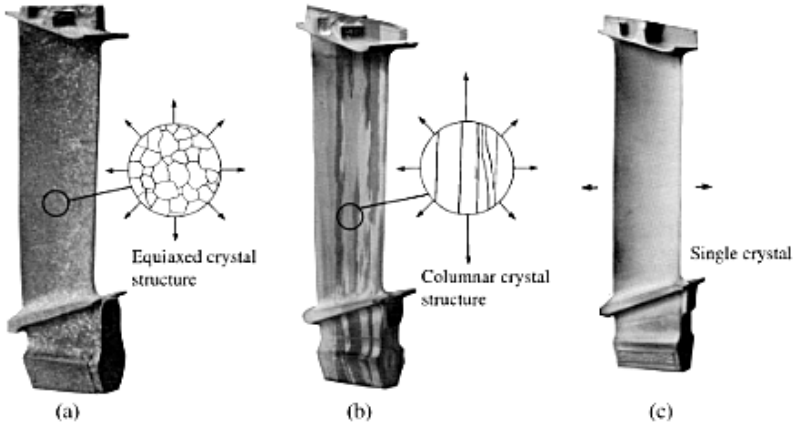

Figure 1.2: Turbine Blades: a) conventionally cast b) directionally solidified and c) single crystal [8].

1.3 Microstructure of Nickel-based superalloys

Nickel superalloys can have a very complex composition and consists of five to ten other elements. The chemical composition determines not only the mechanical properties, but also the corrosion and oxidation resistance. Moreover, the microstructure of nickel superalloys consists of two main phases: γ phase and γ' phase. Since both Phases γ and γ' are coherent, they are in the same crystal orientation, thus there are no grain boundaries, but there are phase boundaries.

γ is a solid solution, containing the basic element Ni and additives of Co, Cr, Mo, Ru, Re [8]. All elements mentioned above have similar atomic radii and the γ-phase, like nickel itself, crystallises in a face-centered cubic (FCC) crystal structure [6, 8]. This phase forms a continuous matrix.

The addition of elements with larger atomic radii such as Al, Nb, Ta and Ti leads to formation of a precipitation phase, the γ' phase. Only a limited volume of the alloying elements can be dissolved into the γ matrix and form a solid solution. As the content of additives increases, the precipitation phase forms [6]. The γ'-phase is an eutectically formed intermetallic phase. It has the theoretical composition Ni_3Al and crystallises in the ordered $L1_2$ structure [6]. The lattice parameters of γ and γ' are very similar, i.e. they are coherent phases [8, 9]. The precipitation of the second phase leads to an increase in the strength of the material [73].

γ' precipitates can grow due to Ostwald ripening [9,73]. In addition, the material can gain further strength through solid solution hardening and grain size strengthening [6].

As can be seen in figure 1.3 the microstructure looks like a brick pattern: γ' phase as dark rectangles (dominant of the volume) and γ phase as bright channels [9].

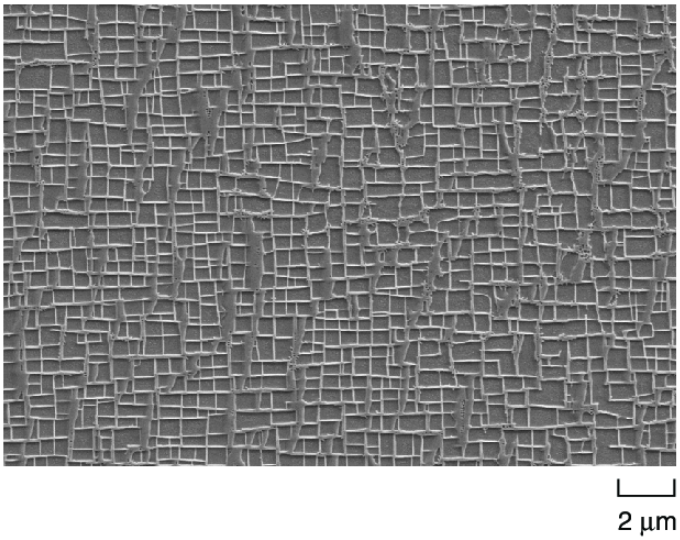

Figure 1.3: Microstructure of the single-crystalline nickel-based superalloy consisting of γ' phase as dark rectangles (dominant of the volume) and γ phase as bright channels [10].

1.4 Corrosion

Corrosion is defined as the reaction of a material with its environment that causes a measurable change in the material and can lead to degradation of the material. Corrosion does not necessarily have to be an undesirable reaction, because corrosion is also understood to be the chemical transformation of a material where the function of the component is not changed. An example of this is the reaction of a metallic surface with its environment and the resulting metal oxide layer, also called a passive layer, which acts as a barrier to further reactions between the metal and the environment. Thermodynamics describes which reaction products are stable and at equilibrium with the environment. The reaction proceeds to minimize Gibbs energy. Kinetics describes the rate at which these products are formed.

The corrosion mechanisms strongly depend on the environmental influences. The most common cause of damage is electrochemical mechanism, i.e. corrosion in an aqueous medium.

This is a redox reaction, where the transfer of electrons takes place at the electrolyte/metal interface. Corrosion can also be mechanically assisted, for example stress corrosion cracking, erosion corrosion, fretting corrosion, etc.

Another mechanism for corrosion occurs in the absence of aqueous media, but in the presence of another elektrolyte, namely molten salts. Other mechanisms are corrosion by liquid metals and hot corrosion. The latter describes corrosion processes at temperatures above the existence of aqueous electrolytes, i.e. corrosion in hot gases, in melts and under hot deposits. This type of corrosion is described in more detail in chapter 1.5.

Corrosion processes can be classified not only according to the respective corrosion media, but also according to the appearance. An example of this would be uniform corrosion, where the entire surface corrodes at almost the same rate. In contrast, pitting results in uneven surface removal, which leads to the formation of small cavities and holes. [12]

1.5 Hot corrosion - sulfidation

High temperature corrosion is the reaction of a material with its ambient atmosphere at temperatures above 500°C leading to accelerated degradation of the material [13]. Damage due to high-temperature corrosion often occurs in power generation, petrochemistry and metallurgy. For example, gas turbines, jet engines, coal gasification plants, heat treatment furnaces, fuel cells and catalyst carriers are affected.

Hot corrosion includes oxidation, carburisation, sulfidation, nitridation, ash- and salt-deposit corrosion and molten salt corrosion [14].

Fuel gas consists of a mixture of hydrocarbons and often contains some nitrogen, carbon dioxide, water and high concentrations of sulfur compounds like H_2S [2]. A way to avoid the problem of sulfidation is to remove sulfur-containing compounds in the natural gas. The Claus process [15] or Hydrodesulfurization (HDS) [16] are two methods of removing sulfur, but both methods are expensive. The sulfidation shows numerous analogies to oxidation in terms of its mechanisms. However, it takes place at a higher speed and can thus result in rapid degradation. Conversely, some metals that show catastrophic oxidation are characterized by quite good resistance under sulfidation conditions, such as the refractory metals W and Mo. The reason for a higher reaction speed for most metals (iron, nickel, cobalt and their alloys with chromium and aluminium) is that the lattice defects of sulfides

are present in a higher concentration than those of the corresponding oxides [17,18].

The kinetics of the sulfide formation can be described with a linear or a parabolic rate law. More severe sulfidation starts when sulfides melt. Since some metals form low melting eutectics with sulfur, the reaction rate with sulfur is also higher [18].

The Ellingham-Richardson diagram of sulfides is depicted in figure 1.4. They are an important tool for assessing the stability of metals in the presence of gases. The Gibbs free energy ΔG^0 is plotted as a function of the temperature for the respective reaction. The slope of the $\Delta G^0(T)$-curves results from the first derivative of the function for the change of state

$$\Delta G^0 = \Delta H^0 - T\Delta S^0 \tag{1.1}$$

which is identical with the entropy change. In an alloy, the element with the highest energy release is sulfidised selectively.

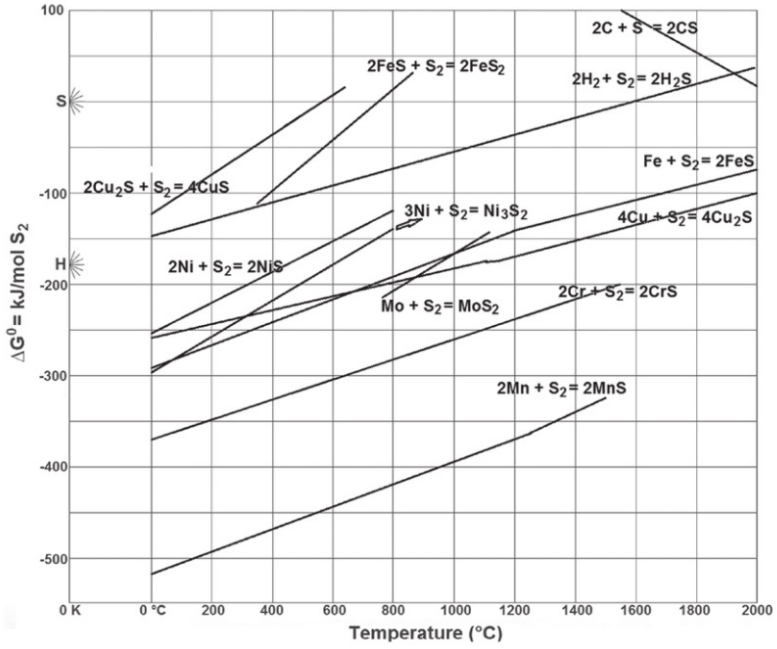

Figure 1.4: Ellingham diagram of sulfides [61]

In contrast to oxidation, where an aluminium oxide and chromium oxide layer are selectively formed, that have a protective effect, the sulfide layers have no protective effect. The Pilling Bedworth Ratio (PBR) gives an indication of whether the sulfide layer can be protective.

The PBR has to be between 1 and 2 to ensure a continuous scale formation and thus form a protective layer. The case that the PBR is < 1 does not occur for sulfides. However, with PBR $>> 1$, spallation and thus material removal must be expected (examples for PBR: NiS 2.5; FeS 2.57; MnS 2.95) [4, 13].

Depending on the sulfur and oxygen activity, different stable phases are formed: NiO when oxygen activity is higher than sulfur activity and $NiSO_4$ when both activities are high [18]. Another problem with sulfur is that it segregates between the metal and oxide interface, which leads to spallation of the protective oxide layer [20].

The thermal stability of the materials would often be sufficient, but the presence of corrosive species such as salt deposits increases the corrosive severity immensely. Since NaCl (contained in sea salt) is unstable in the presence of sulfur at high temperatures, the salt reacts with SO_3 and leads to the formation of the corrosive agent sodium sulfate Na_2SO_4 [21].

$$2\,NaCl_{(s)} + SO_{3(g)} + \frac{1}{2}\,O_{2(g)} \rightleftharpoons Na_2SO_{4(s)} + Cl_{2(g)} \tag{1.2}$$

Other possible reactions are [22]:

$$2\,NaCl_{(s)} + SO_{3(g)} + H_2O_{(g)} \rightleftharpoons Na_2SO_{4(s)} + 2\,HCl_{(g)} \tag{1.3}$$

$$2\,NaCl_{(s)} + SO_{2(g)} + O_{2(g)} \rightleftharpoons Na_2SO_{4(s)} + Cl_{2(g)} \tag{1.4}$$

The molten Na_2SO_4 partially decomposes into NaO_2 and SO_3 according to the following equation:

$$Na_2SO_4 \rightleftharpoons Na_2O + SO_3 \tag{1.5}$$

Hot corrosion takes place in two stages: initiation stage and propagation stage. During the initiation stage, the oxide layer on the material remains protective and the salt deposit has no influence on the corrosion rate [21].

During the propagation stage, the salt deposit reacts with the protective oxide layer and leads to the dissolution of the protective layer. A distinction is made between two propagation modes: basic and acidic fluxing. The content ratio between Na_2O and SO_3 in the melt (see equation 1.5) determines the basicity of the melt and depending on this, one of the two corrosion mechanisms, basic or acidic fluxing, takes place.

Assuming that the protective oxidation layer is NiO, basic fluxing dissolves the protective layer with the help of oxide ions:

$$NiO_{(s)} + O^{2-} \rightleftharpoons NiO_2^{2-} \tag{1.6}$$

In contrast, the dissolution of the NiO layer in acidic fluxing proceeds according to the following equation:

$$NiO_{(s)} \rightleftharpoons Ni^{2+} + O^{2-} \tag{1.7}$$

A distinction is made between 2 types of hot corrosion [23]:

- High temperature hot corrosion type I (HTHC): typically beween 750 – 900°C.
  HTHC takes place between the melting point of the surface deposit and vapor deposition dew point for the salt deposit, i.e. in the liquid state of salt slag deposits. In this type of hot corrosion, the sodium sulfate is reduced to sulfur and diffuses into the bulk of the material, causing damage [24].
- Low temperature hot corrosion type II (LTHC): typically between 600 – 750°C.
  In the case of LTHC, a salt mixture in solid state reacts with the material surface and a low-melting (631°C [25]) eutectic is formed, for example Na_2SO_4 – $NiSO_4$. A sufficiently high partial pressure of SO_3 is necessary for the stabilisation of nickel sulfate [26]. This form of corrosion damage is characterized by the appearance of pitted or uneven surfaces [23].

Chapter 2

SO_3 Formation

During the combustion of fossil fuels the hydrogen sulfide H_2S contained in raw gas is first oxidised to SO_2 and then to SO_3. In the combustion gas the concentration of SO_2 is several orders of magnitude higher than that of SO_3 [28].

$$SO_2 + \frac{1}{2}\,O_2 \rightleftharpoons SO_3 \tag{2.1}$$

While SO_2 is relatively benign, the SO_3 gas leads to rapid degradation of the material of the turbine blades, i.e. the nickel alloys [31]. The reaction of pure Ni with a gas mixture of SO_2 + O_2 and SO_3 leads to the formation of NiO and $Ni_{3\pm x}S_2$. The resulting NiO reacts with SO_3 to form $NiSO_4$. The outwardly diffusing nickel reacts with $NiSO_4$ [32]:

$$9\,Ni + 2\,NiSO_4 \rightleftharpoons 8\,NiO + Ni_{3\pm x}S_2 \tag{2.2}$$

The formation of SO_3 depends on several parameters such as the concentration of SO_2, O_2, NO_x, temperature, moisture content, presence of catalysts, etc. [28].

2.1 Effect of temperature

As far as the influence of temperature is concerned, the formation of SO_3 is thermodynamically preferred when the gas is cooled down (below 700°C [33]). Simultaneously, however, the reaction takes place only slowly at low temperatures [34]. At a temperature inter-

val of 400 - 700°C the SO_3 concentration is higher, the higher the temperature [35]. The formation of SO_3 is described as "sluggish" but is thermally activated and promoted by the presence of catalysts [29, 30]. The following figure 2.1 shows the opposite influence of thermodynamics [35] and kinetics [36]. The blue line shows that the formation of SO_3 is thermodynamically favoured below 400°C, whereas the formation of SO_2 is favoured from 900°C onwards.

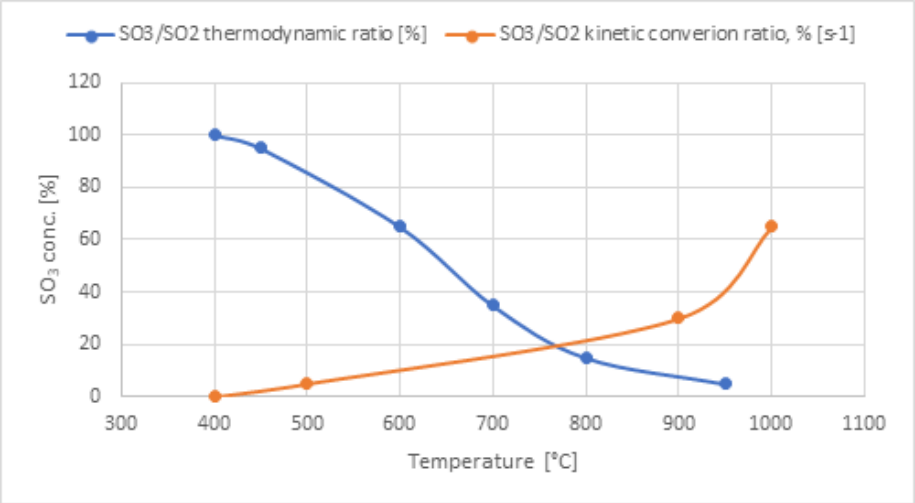

Figure 2.1: SO_3/SO_2 conversion ratio [35, 36].

At higher temperatures (above 900°C [35]), the SO_2 is oxidised directly with O radicals [38] (primary oxidation of SO_2):

$$SO_2 + O(+M) \rightleftharpoons SO_3(+M) \tag{2.3}$$

Whereas at lower temperatures the oxidation takes place via $HOSO_2$ formation [29, 32, 39] (secondary formation of SO_3), as $HOSO_2$ is not stable above 700°C [35]:

$$SO_2 + OH(+M) \rightleftharpoons HOSO_2(+M) \tag{2.4}$$

$$HOSO_2 + O_2 \rightleftharpoons SO_3 + HO_2 \tag{2.5}$$

SO_3 is mainly consumed by the following reaction:

$$SO_3 + H^{\bullet} \rightleftharpoons SO_2 + OH \tag{2.6}$$

As the below listed reaction is too slow to be significant [32]:

$$SO_3 + O^{\bullet} \rightleftharpoons SO_2 + O_2 \tag{2.7}$$

2.2 Effect of moisture

Since sulfur trioxide is a hygroscopic material, it reacts with water to form gaseous sulfuric acid [28]. The conditions for the formation of H_2SO_4 are the presence of moisture and a temperature below 500°C [40]. Since the combustion of hydrocarbons contained in the fuel leads to water and carbon dioxide, presence of moisture is unavoidable. If the temperature drops below 200°C all SO_3 molecules are converted into sulfuric acid [38].

$$SO_{3(g)} + H_2O_{(g)} \rightleftharpoons H_2SO_{4(g)} \tag{2.8}$$

Below acid dew point the gaseous sulfuric acid condenses and forms drops and films on the material, which may lead to rapid corrosion. The higher the concentration of SO_3 and H_2O, the higher the acid dew point [29, 41]. The acid dew point temperature can vary between 95°C and 160°C [42]. This low temperature corrosion can be counteracted by keeping the temperature above the acid dew point. Since liquid sulfuric acid together with water forms an azeotrope, the composition of the condensate differs from that of the gas phase [39].

The higher the water content in the system, the higher the concentration of SO_3. This is due to the formation of OH radicals, that subsequently reacts via $HOSO_2$ formation to SO_3 as shown in equation 2.9 [40].

$$H_2O + O^{\bullet} \rightleftharpoons OH^{\bullet} + {}^{\bullet}OH \tag{2.9}$$

According to *Duan et al.* [35] as the moisture content increases from 5% to 15%, the SO_3 concentration simultaneously increases from 3.7ppm to 7.1ppm. In many measuring experiments the water is removed to avoid the formation of sulfuric acid. The problem is that the water content also has an influence on the SO_2-SO_3 equilibrium. In case the moisture is removed the equilibrium shifts towards SO_2.

2.3 Impact of O_2, SO_2, CO_2 and NO concentration

The higher the SO_2 concentration, the higher is the SO_3 concentration [38, 42]. Furthermore, the O_2 concentration also increases the SO_3 content, since more molecular oxygen is available [35]. The O_2 concentration only has an influence in a range of 3-10 Vol-% [42]. Further increment of the O_2 concentration has no influence on the SO_3 concentration [35].

According to Duan et al. [35] CO_2 has no influence on SO_3 formation, whereas according to Fleig et al. [34] CO_2 promotes the formation of SO_3 at higher temperatures. According to Wendt and Sternling [45], the formation of SO_3 is catalytically promoted by NO. At product quantity above 10^{-7} mole the following reactions takes place:

$$2\,NO + O_2 \rightleftharpoons 2\,NO_2 \tag{2.10}$$

$$NO_2 + SO_2 \rightleftharpoons SO_3 + NO \tag{2.11}$$

At lower concentration, reaction 2.10 is slow. Instead, reaction 2.12 proceeds:

$$NO + O_2 \rightleftharpoons NO_3 \tag{2.12}$$

whereupon the following reaction takes place:

$$NO_3 + SO_2 \rightleftharpoons SO_3 + NO_2 \tag{2.13}$$

and reaction 2.10.

NO_x reduction catalysts used to reduce NO_x emissions typically increase SO_3 concentrations [34, 46]. NO_x is also selectively catalytically reduced (SCR) using ammonia over catalysts. In case of an ammonia slip, NH_3 reacts with SO_3 to ammonium bisulfate (NH_4HSO_4) or ammonium sulfate ($(NH_4)_2SO_4$), which contributes to PM_{10} (particulate matter with a diameter of 10 μm) emissions [47–49].

2.4 Catalytic effect of fly ash and Platinum

In corrosion tests, according to Kofstad [18], a higher weight increase of Ni samples by the formation of corrosion products was found when using Pt catalysts at a temperature of 700°C, since the reaction $SO_2 \rightarrow SO_3$ is accelerated by using Pt catalysts. The metal oxides contained in the fly ash influence the formation of SO_3. Compared to the other metal oxides, Fe_2O_3 has the strongest effect [43, 47] in promoting the oxidation of SO_2 to SO_3, but also V_2O_5 proves to be a good catalyst for SO_3 formation [38]. An increasing content of Fe_2O_3 leads to an accelerated formation of SO_3 [42, 50]. It was found by Marier and Dibbs [50] that 700°C is the temperature where SO_3 is most effectively produced. Alkali- and Alkaline earth metal oxides such as CaO and MgO capture the SO_3 and form sulfates [42, 50]. The carbon contained in the fly ash acts as oxygenscavenger and therefore inhibits SO_3 formation [50].

Chapter 3

SO_3 Measurement Techniques

The measurement of SO_3 is by no means trivial since SO_3 is a highly reactive gas and not easily differentiated from SO_2. While measuring the SO_3 concentration the occurrence of reactions must be avoided until the gas reaches the detector. Furthermore, as can be seen in the chapter above, moisture and temperature have great influence on the equilibrium. Below 500°C and in the presence of water, SO_3 is consumed to form sulfuric acid. Condensation of the gases is also an obstacle to correct measurement.

The low SO_3 concentration makes the measurement more complicated and furthermore the parent molecule SO_2, which is present in a higher concentration, interacts with SO_3 and is therefore a disruptive factor. The differentiation of SO_2 and SO_3 is quite difficult, hence to this day only SO_x is being determined rather than the individual gases separately [34].

3.1 Satellite Measurement

Currently, satellite measurement methods are not able to distinguish SO_2 from SO_3 and are therefore not suitable for determining SO_3 contents only. Nevertheless, since stationary gas turbines from Solar Turbines are installed all over the world for power generation, it is very useful to know in which regions the SO_x concentration is particularly high due to volcanic activity or the emission from smelters. This applies to gas turbines in general and therefore also applies to other companies and aviation safety.

The Total Ozone Mapping Spectrometer TOMS, as the name suggests, was installed on a satellite called Nimbus 7 to measure ozone. After the eruption of El Chichon 1982, the

measurement of SO_2 had also started, for which the TOMS algorithm had to be modified.

Since SO_x emissions from lower altitudes, caused by smelters, are much more difficult to measure than emissions caused from volcanoes at higher altitudes, hyperspectral instruments were introduced [51, 52].

The following figure 3.1 shows recent SO_x images from NASA.

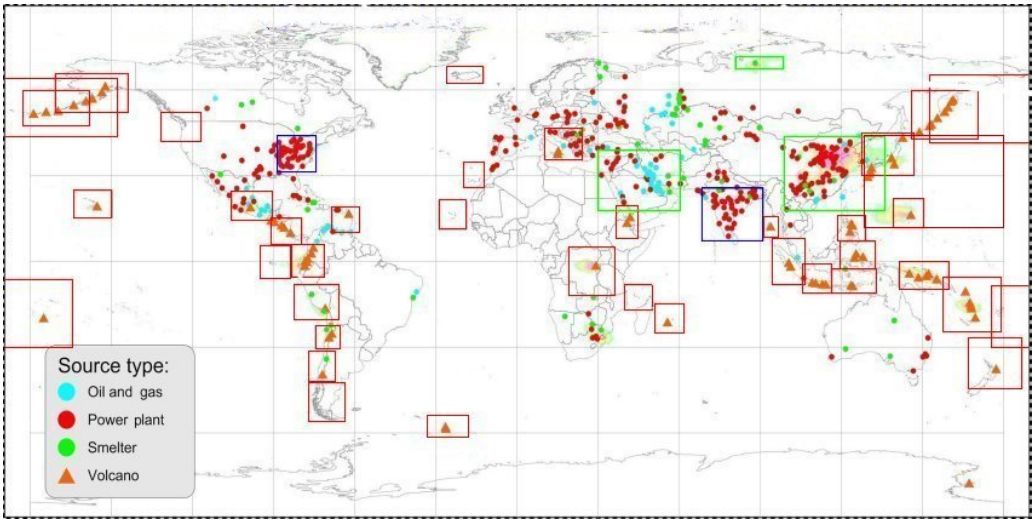

Figure 3.1: World risk map from NASA depicting SO_2 concentration [52].

ESA has developed an UV-VIS-NIR-SWIR spectrometer called Tropomi, which is on the satellite called Sentinel5. It can measure ozone, NO_x, CO and aerosols as well as SO_x in a vertical column distribution. A complex environmental model is therefore needed to determine with precision the altitude of the sulfur dioxide cloud. [54].

3.2 Wet chemical analysis

In chemical analysis, mostly the quantity of gaseous sulfuric acid is determined, which is proportional to the content of SO_3. If sulfuric acid is to be used to measure SO_3, it means that moisture must be present to convert SO_3 to H_2SO_4 (see equation 2.8) and the temperature must be set to the H_2SO_4 formation temperature (below 500°C) [40].

In most cases, the SO_3 or H_2SO_4 contained in the gas is converted to sulfate ions. Subsequently the concentration of the ions can be determined by ion chromatography or titration

with barium perchlorate and thorine as indicator and thus the SO_3 concentration determination can take place.

3.2.1 Controlled Condensation Method

As the name implies, the gaseous sulfuric acid is condensed in a controlled manner, avoiding the condensation of water by cooling the gas between the acid dew point and the water dew point. This corresponds to a temperature between 80°C and 90°C [55]. The schematic structure is depicted in figure 3.2.

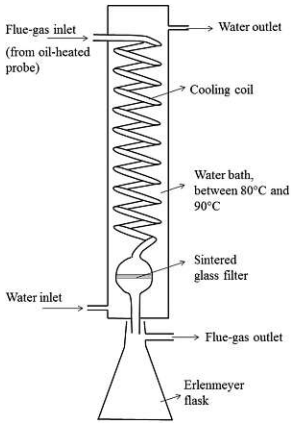

Figure 3.2: Design of glass cooler used in Controlled Condensation Method setup for SO_3 concentration measurement [34].

The condensed sulfuric acid is adsorbed on the walls of the cooling coil and in the glass filter [34,44,56]. The SO_3 or H_2SO_4 is absorbed by an aqueous isopropanol solution $(CH_3)_2CHOH$ with a specific pH value of 4.6 [56]. The gases are dissolved as sulfate ions SO_4^{2-}, which can then be determined by ion chromatography [44].

According to *Maddalone et al.* [55] the measurement is well reproducible with a variation coefficient of ±6%, but they also state a much lower accuracy for field tests.

3.2.2 Salt Method

The principle of the salt method is based on flowing gas above the acid dew point through a bed of salt in a Teflon tube. In this process the aerosol H_2SO_4 or gaseous H_2SO_4 reacts with the salt, thus avoiding losses in the sampling line due to undesired condensation.

This analytical method was first described by Kelman [57], who used sodium chloride as a salt. The following reactions occur between NaCl and gaseous H_2SO_4 (see equation 2.8

$$NaCl_{(s)} + H_2SO_{4(g)} \longrightarrow NaHSO_{4(s)} + HCl_{(g)} \tag{3.1}$$

$$2\,NaCl_{(s)} + H_2SO_{4(g)} \longrightarrow Na_2SO_{4(s)} + 2\,HCl_{(g)} \tag{3.2}$$

$$NaHSO_{4(s)} + NaCl_{(s)} \longrightarrow Na_2SO_{4(s)} + HCl_{(g)} \tag{3.3}$$

The resulting sodium bisulfate or sodium sulfate is then dissolved in deionized water and the sulfate ions are analysed by ion chromatography. Sodium bisulfate tends to form at lower temperatures, whereas the reaction of sodium sulfate production takes place at higher temperatures [34].

Yuzhong Li et al. [56] analysed a gas mixture consisting of sulfuric acid, nitrogen and oxygen and excluded the gases SO_2, CO_2 and NO_x. The measurement was well reproducible with a variation coefficient of $\pm 5\%$, but his experiments did not show any correlation of SO_2 and SO_3 interferences [34, 55, 58, 59].

Vainio et al. [44] have also experimentally tested other salts, instead of NaCl, for the analysis of SO_3, namely KCl, K_2CO_3, and $CaCl_2$. It turned out that only NaCl and KCl are suitable for the analysis, since this undesired reaction 3.4 takes place very slowly [34]:

$$4\,NaCl_{(s)} + 2\,SO_{2(g)} + 2\,H_2O_{(g)} + O_{2(g)} \longrightarrow 2\,Na_2SO_{4(s)} + 4\,HCl_{(g)} \tag{3.4}$$

The salts K_2CO_3 and $CaCl_2$ capture too much SO_2 and therefore the determined SO_3 concentration is too high. On the contrary, a big advantage of the salt method when using NaCl or KCl is that there is only little interference of SO_2 when measuring SO_3. Furthermore, compared to the above described Controlled Condensation Method, the salt method is a cheaper and simpler method of analysis [60]. *Fleig et al.* [28] have also tried to measure the SO_3 content continuously and indirectly by measuring the HCl content using a Fourier-transform infrared spectroscopy (FTIR). The problem is that in the formation of sodium bisulfate the ratio of H_2SO_4 to HCl is 1:1, whereas in the formation of sodium sulfate the ratio of H_2SO_4 to HCl is 1:2 [58].

As shown in figure 3.3 [34] the setup was designed to measure the SO_2 concentration simultaneously by flowing the gas through two impingers filled with H_2O_2 where the SO_2 oxidized to sulfate ions. The concentration of sulfate ions was determined by titration with

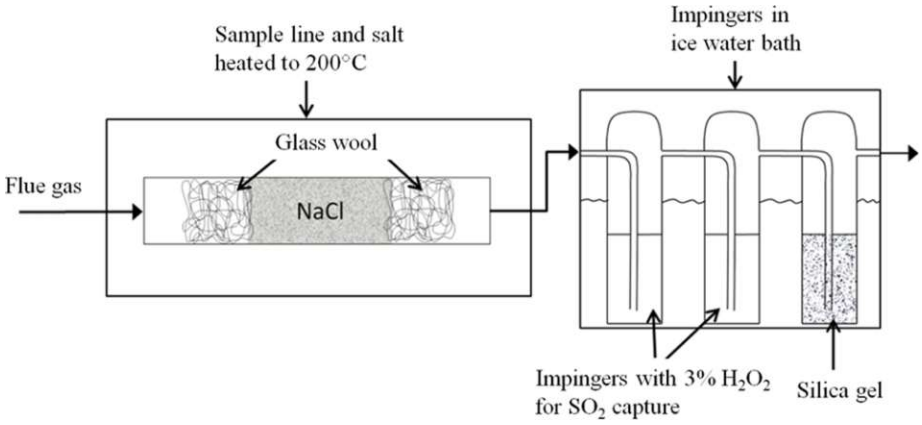

Figure 3.3: Design of Salt method setup for simultaneous SO_2 and SO_3 measurement [34].

barium perchlorate and thorine as an indicator [34, 58].

3.2.3 Isopropanol Absorption Method

This method is based on the Test Method 8 of the Environmental Protection Agency (EPA) [72]. As depicted in figure 3.4 [34] the Isopropanol absorption method is a setup where the gas is first passed through an impinger filled with 80% isopropanol solution diluted in water to dissolve the SO_3 and H_2SO_4 and then through two impingers filled with H_2O_2 to capture the SO_2 contained in the gas. At the end there is an impinger with silica gel to absorb the moisture from the gas [34]. The impingers are placed inside an ice bath to effectively capture SO_3 and SO_2.

To remove any unwanted dissolved SO_2 from the isopropanol, it is recommended to bubble argon through the solutions after the sampling [61]. Additionally, to avoid dissolving SO_2 in the solution, the pH value should be slightly acidic [62] The isopropanol solution and H_2O_2 solution are analysed separately.

The amount of sulfate ions formed in the isopropanol solution is determined by adding thorin indicator to the solution and titrating with barium perchlorate. The SO_2 reacts with H_2O_2 and oxidizes to sulfate ions,which can likewise be titrated with barium perchlorate and thorin as indicator.

A possible error in this method could be the absorption and oxidation of SO_2 to SO_3 in the isopropanol solution [58].

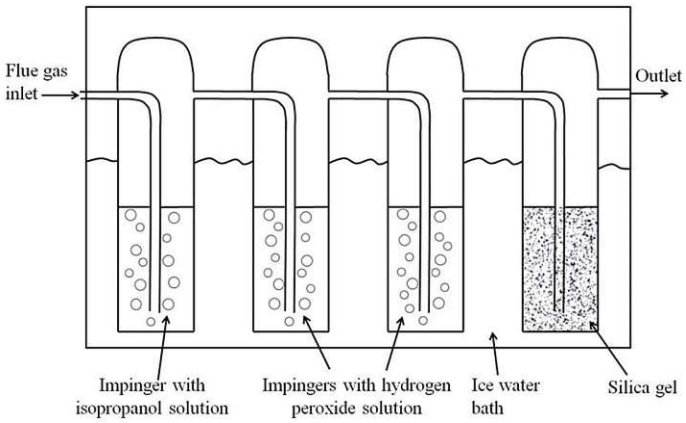

Figure 3.4: Design of Isopropanol Absorption Method setup for simultaneous SO_2 and SO_3 concentration measurement [34].

3.2.4 Pentol SO_3 Monitor

Pentol SO_3 Monitor is the only method amongst the wet chemical analysis methods that is a continuous measurement technique. This method was first described by *Jackson et al.* [63]. As shown in figure 3.5 [34] isopropanol drips onto flowing gas and the SO_3 or H_2SO_4 are absorbed as sulfate ions. Barium chloranilate is added to the solution and the following reaction takes place.

$$SO_4^{2-} + BaC_6O_4Cl_2 + H^+ \longrightarrow BaSO_4 + HC_6O_4Cl_2^- \tag{3.5}$$

The resulting chloroanilite ions produce a violet solution and are determined in a continuous and automated manner. The ions absorb light at 535nm, which is determined with a photometer. The higher the absorption, the higher the concentration of chloranilite ions. The concentration of the ions is proportional to the SO_3 content [34].

Compared to the controlled condensation method, the accuracy of the Pentol SO_3 Monitor is lower, but may still be suitable if continuous measurement is required. The reason for the lower accuracy might lie in the fact that SO_2 is absorbed by isopropanol [58, 62].

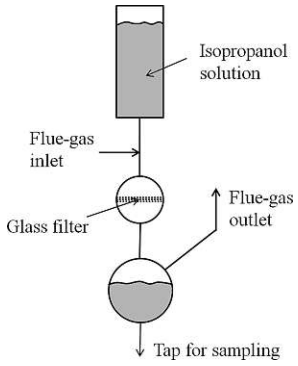

Figure 3.5: Design of Pentol SO_3 Monitor method setup for SO_3 concentration measurement [34].

3.2.5 Acid Dew-Point Meter

In the acid dew point method, the sulfuric acid contained in the gas is condensed onto a surface in a controlled manner. The resulting acid film is highly conductive, and the aim is to determine the conductivity together with the temperature. Nowadays, there are portable acid dew point meters available, that contain a probe consisting of a ring electrode made of pure platinum and a Pt-PtRh thermocouple for temperature measurement [34, 64]. When evaporation and condensation are in equilibrium, the flowing current is constant, and the temperature measured corresponds to the acid dew point [61]. The SO_3 concentration can be calculated from the determined dew point temperature, H_2O content and the pressure of H_2O and SO_3 [61]. During the measurement, it is important to make sure that the sensor is clean because particulate matter and salt deposits falsify the conductivity measurement [61]. The determination of the SO_3 content using this method is difficult since errors can occur during the determination itself and uncertainties can arise during the calculation [61].

3.2.6 Indirect SO_3 measurement via CO_2 formation

In this method gaseous SO_3 is determined indirectly by reacting with calcium oxalate CaC_2O_4 to form CO_2:

$$SO_{3(g)} + CaC_2O_{4(s)} \longrightarrow CaSO_{4(s)} + CO_{2(g)} + CO_{g)} \tag{3.6}$$

The resulting CO_2 is determined by IR spectrometry and simultaneously the SO_2 contained

in the gas is determined by UV spectrometry. According to Ibanez et al, the interference with SO_2 is low in this method because the CaC_2O_4 reacts selectively with SO_3 [65].

3.3 Fourier-transform infrared spectroscopy (FTIR)

The FTIR measurement is very challenging due to the difficult gas handling. Losses of SO_3 can occur very easily due to high reactivity of SO_3. For example, if moisture is present, SO_3 reacts to H_2SO_4 and is therefore not detectable. For this reason, only chemically inert materials such as teflon or quartz should be used in the measurement to avoid side reactions in the sampling line [38,49]. InSb- and mercury cadmium telluride (MCT) detectors can be used as detectors and measurements can be made in absorption mode as well as in emission mode. Two SO_3 bands are visible in the FTIR spectrum:

- a stronger band at about 1386cm^{-1}, but here there is an interference with SO_2 and H_2O bands
- a weaker band at 2438cm^{-1}. The big challenge is that this band is 66 times weaker than the band at 1386cm^{-1} and the SO_3 concentration is already much lower than the SO_2 concentration. This is still the more attractive band since there is only an overlap with a weak CO_2 band, but this can be handled [49].

Fateev et al. [49] have used in situ produced SO_3 gas for the determination of the SO_3 content using FTIR to ensure easier gas handling. He did this by reacting either SO_2 with ozone or SO_2 with O_2 over a platinum catalyst. He has also removed all moisture from the system to avoid sulfuric acid formation. However, the removal of the water causes a shift in the equilibrium towards SO_2 (equation 2.9). All measures taken to be able to determine the SO_3 content, for example the removal of moisture, lead to a change in the analyte. The determination of SO_3 using FTIR is therefore only possible to a limited extent under certain conditions and can't be used for a field test.

3.4 Mass spectroscopy

To ensure a successful measurement, supersonic molecular beam sampling must be used so that the gas can be transported into the ionisation chamber without condensation or reaction [34].

3.5 Summary of analytical methods

Table 3.1 shows an overview of the measurement methods listed above.

Table 3.1: Comparison between the different measurement methods.

Method	measured gas	advantages	disadvantages
Satellite Measurement [51, 52]	SO_2 + SO_3	reliable SO_x measurement technique	No distinction between SO_2 and SO_3
CCM [34, 55]	H_2SO_4	well reproducible	exact temperature setting between 80 and 90°C necessary
Salt [34, 44, 56, 57]	H_2SO_4 + SO_3, SO_2	cheaper and simpler than CCM	direct SO_3 measurement not possible
IPA [34, 61, 62]	H_2SO_4 + SO_3, SO_2	direct measurement of SO_3 possible	positive bias towards SO_3 possible
Pentol Monitor [34, 62, 63]	H_2SO_4 + SO_3	continuos measurement technique	lower accuracy
Acid-Dew-Point-Meter [34, 61, 64]	H_2SO_4	portable acid-dew-point meters available	many sources of error
Indirect SO_3 Measurement [65]	CO_2	low interference with SO_2	a lot of effort
FTIR [49]	SO_3		difficult gas handling, removal of moisture necessary, etc.
Mass Spectroscopy [34]	SO_3		difficult gas handling

Chapter 4

Modelling

Since it is very complex to determine the SO_3 content experimentally, modelling was the first step. In the following chapter, the SO_2-SO_3 equilibrium was simulated and thus the influence of different conditions was simulated.

4.1 Chemical Equilibrium with Applications CEA

The CEA is a computer program that was developed by NASA Lewis Research Center about 40 years ago and has been continuously improved since then, for example by taking advantage of improved computer capabilities and by adding new features.

With the help of this program, chemical equilibria can be calculated from any reactant. For this purpose, one must assign two thermodynamic state functions in each case. The following options are available:

- tp: temperature and pressure
- hp: enthalpy and pressure: gives constant-pressure combustion properties
- sp: entropy and pressure
- tv: temperature and volume (or density)
- uv: internal energy and volume: gives constant-volume combustion properties
- sv: entropy and volume (or density)

Moreover, with the help of CEA [66] theoretical rocket performance for a combustion chamber, Chapman-Jouguet detonations and shock tube parameters for incident and reflected shocks can be calculated.

Chemical equilibria can be calculated either using equilibrium constants or by minimizing the free energy. The minimization of free energy has the great advantage that each species can be treated independently and one does not have to describe reactions in advance, which is why this is the method used for the calculation here.

As the system moves from the initial state to the state of equilibrium, its composition changes and with it its entropy. The state of equilibrium is reached at that composition at which the total entropy has the highest value (Second Law of Thermodynamics). In the case that temperature and pressure are used to describe the thermodynamic state (tp), the condition of maximum entropy of the system is equivalent to the condition of minimum Gibbs energy of the system. The equilibrium composition can therefore be determined by minimising the Gibbs energy. In the case where temperature and volume are used to describe the thermodynamic state (tv), the equilibrium composition can be determined by minimising the Helmholtz energy [66].

4.1.1 CEA Results

For the modelling of the SO_2-SO_3 equilibrium, the thermodynamic states temperature and pressure (1bar) (tp) were assigned. The temperature for the calculation was mostly set between 400 and 1100°C. The CEA programme also requires a well-defined temperature at which the fuel enters the combustion chamber and was set to 100°C for this purpose.

Effect of temperature

Input: Mole fractions: 0.021 SO_2, 0.206 O_2, 0.774 N_2, p = 1bar

As can be seen in figure 4.1, formation of SO_3 is favoured at low temperatures, which is consistent with the literature. As already described in chapter 2.1, the formation of SO_3 below 700°C [33] is thermodynamically favored. The same could be shown with the help of this modelling.

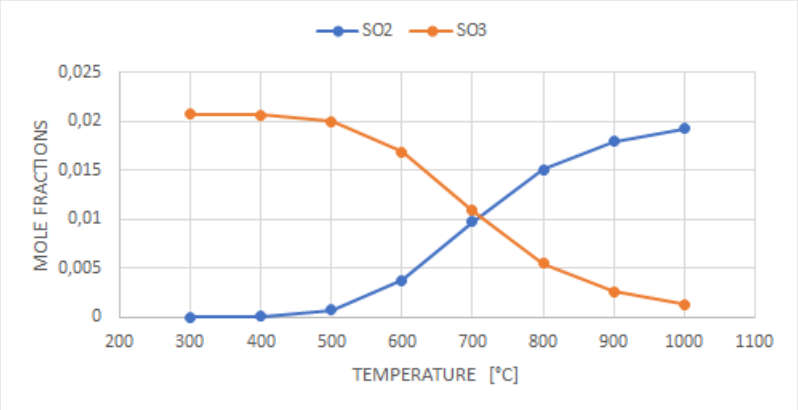

Figure 4.1: Effect of Temperature (CEA).

Effect of CO_2 and SO_2

As can be seen in figure 4.2 the CEA modelling could confirm that the higher the SO_2 concentration, the higher is the SO_3 concentration [38, 42].

Input (1000ppm SO_2): Mole fractions: 0.002 SO_2, 0.212 O_2, 0,757 N_2, p = 1bar
Input (5000ppm SO_2): Mole fractions: 0.001 SO_2, 0.21 O_2, 0.789 N_2, p = 1 bar
Input (1v% SO_2): Mole fractions: 0.00022 SO_2, 0.216 O_2, 0.816 N_2, p= 1bar

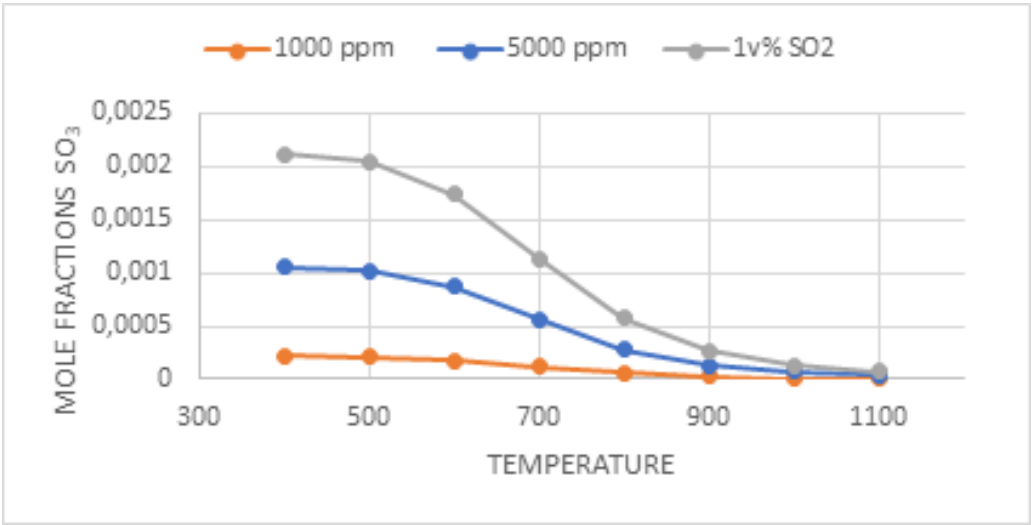

Figure 4.2: Effect of SO_2 (CEA).

According to *Duan et al.* [35] CO_2 has no influence on SO_3 formation, whereas according to *Fleig et al.* [34] CO_2 promotes the formation of SO_3 at higher temperatures. With the help of the CEA programme, it could be determined that CO_2 has no influence on the formation of SO_3 (figure 4.3).

Input: Mole fractions: 0.02 SO_2, 0.202 O_2, 0.757 N_2, 0.02 CO_2; p = 1bar

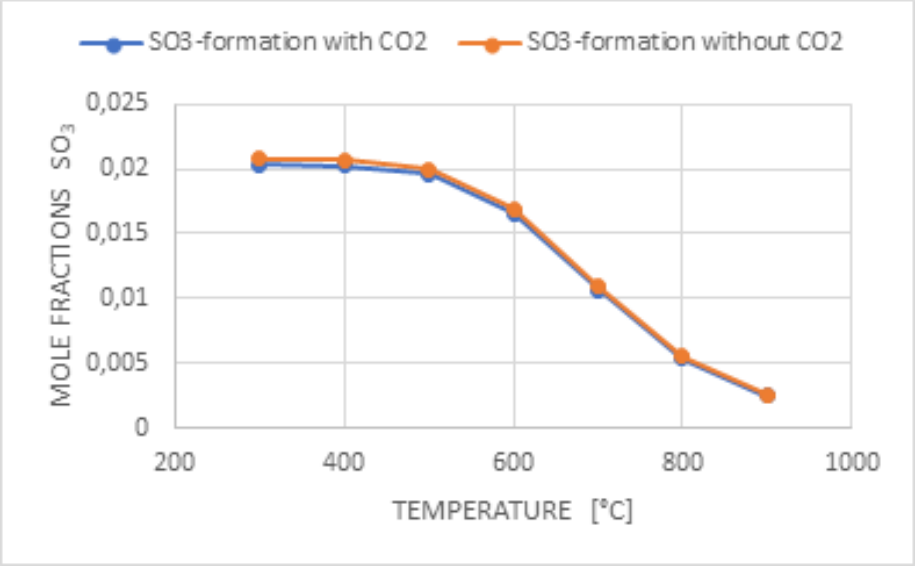

Figure 4.3: Effect of CO_2 (CEA).

Effect of moisture

As can be seen from figure 4.4, the modeling result is congruent with the trends described in the literature (described in chapter 2.2) that sulfuric acid forms at a temperature below 500°C [40] in the presence of moisture. It is also confirmed by these calculation that below 200°C all SO_3 is converted to sulphuric acid [38]. At 100°C there is no SO_3, but the highest content of sulphuric acid is present (4.4). The literature research has shown that the acid dew point is between 95°C and 160°C [42]. In the following figure 4.4, however, it is at about 200°C. Since the acid dew point depends on the concentration of SO_3 and H_2O, the deviation could be due to the different initial composition [29]. Therefore the thermodynamic calculation indicates that it would be advisable to keep the temperature above 400°C to prevent the rapidly progressing corrosion caused by sulphuric acid and especially above 200°C to prevent liquid sulfuric acid to form drops and films on the material.

Input: Mole fractions: 0.02 SO_2, 0.202 O_2, 0.758 N_2, 0.02 H_2O; p = 1bar

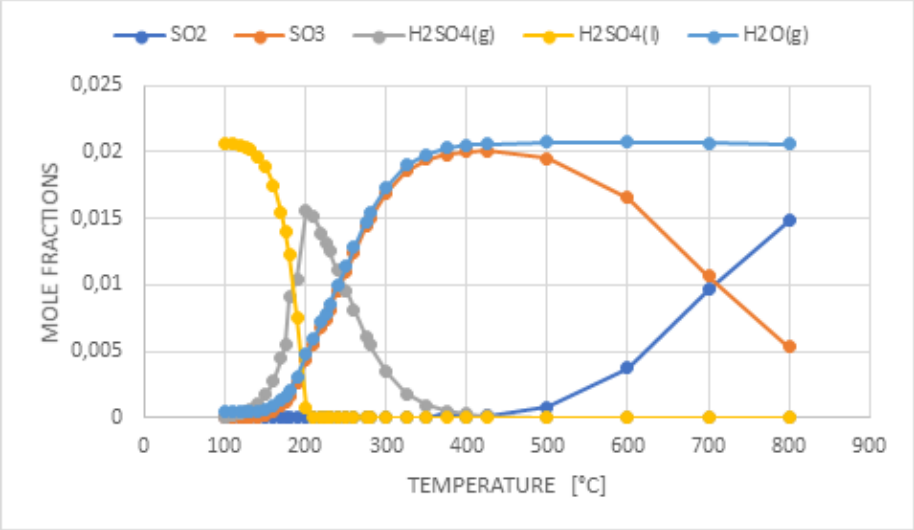

Figure 4.4: Effect of moisture (CEA).

Modelling of gas turbine combustion

In a combustion chamber, combustion stability must be ensured, i.e. no flame extinction or large pressure loss should occur over a wide range of operating conditions. A distinction is made between a rich (high fuel flow, little air flow) and lean (little fuel flow, high air flow) oxygen to fuel (o/f) ratio (mass ratio in grams). An o/f between 50 and 130 is considered a normal operating range. Flame extinction occurs when the turbine is operated beyond this range. The range of air/fuel ratio also depends on the air velocity. A stability loop is shown in figure 4.5, where the air/fuel ratio is plotted as a function of air mass flow.

The gas composition that occurs when H_2S-rich fuel is burnt was simulated using the CEA programme. For the input settings, the hp mode was selected here, i.e. a constant pressure of either 10 bar, 15 bar or 20 bar was set. The ignition temperature was set at 3800K and the temperature at which the fuel enters the combustion chamber was set to 100°C. For the calculation, the following fuel was used: 97% CH_4 and 3% H_2S and the o/f ratio was set to between 40 (full load) and 130 (idle load). The resulting gas composition is shown in the following table 4.1 (10 bar).

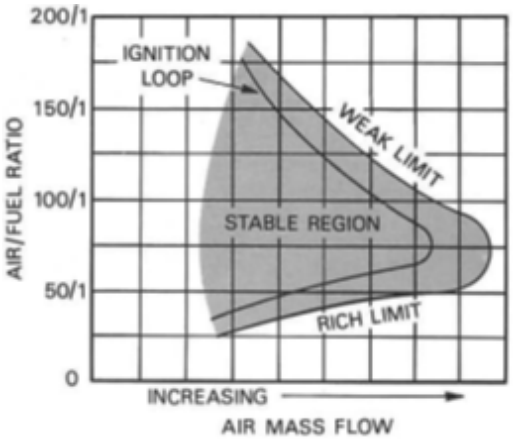

Figure 4.5: Combustion stability loop [67].

Table 4.1: Gas composition after combustion for 10 bar between full load (o/f=40) and idle load (o/f=130).

o/f	Ar	CO_2	H_2O	NO	NO_2
40	0,00897	0,04224	0,08447	0,00048	0,00001
50	0,00905	0,03414	0,06816	0,00017	0,00001
60	0,0091	0,02867	0,05713	0,00006	0,00001
70	0,00914	0,02472	0,04917	0,00003	
80	0,00916	0,02173	0,04316	0,00001	
90	0,00919	0,0194	0,03845	0,00001	
100	0,0092	0,01753	0,03467		
110	0,00922	0,01599	0,03157		
120	0,00923	0,0147	0,02897		
130	0,00924	0,01361	0,02677		

o/f	N_2	O_2	SO_2	SO_3	H_2SO_4
40	0,74763	0,11557	0,00057	0,00004	
50	0,75419	0,1338	0,00039	0,00011	
60	0,75858	0,14605	0,00022	0,00019	
70	0,76173	0,15486	0,00011	0,00025	
80	0,76409	0,16153	0,00005	0,00027	
90	0,76593	0,16675	0,00002	0,00026	
100	0,7674	0,17095	0,00001	0,00024	
110	0,7686	0,17439		0,00022	
120	0,76961	0,17727		0,0002	0,00001
130	0,77047	0,17972		0,00018	0,00001

Figure 4.6 shows graphically the amount of SO_2, SO_3 and H_2SO_4 produced as a function of o/f. The amount of gases produced do not change too much depending on the pressure. At 20bar, compared to 10 bar, less SO_2 is produced, but more SO_3 and H_2SO_4. Under the conditions described above, H_2SO_4 in the order of 100ppm is only formed above an o/f ratio of approx. 110. At an o/f ratio of 130 more SO_3 is produced than at an o/f ratio of 40, since the gas mixture is relatively cool here. However, there is a specific region between the stator and the disc where hot air is mixed with cold, compressed air (after the combustor (figure 1.1)), creating conditions where there is a higher probability of SO_3 formation even at very low values of o/f ratios.

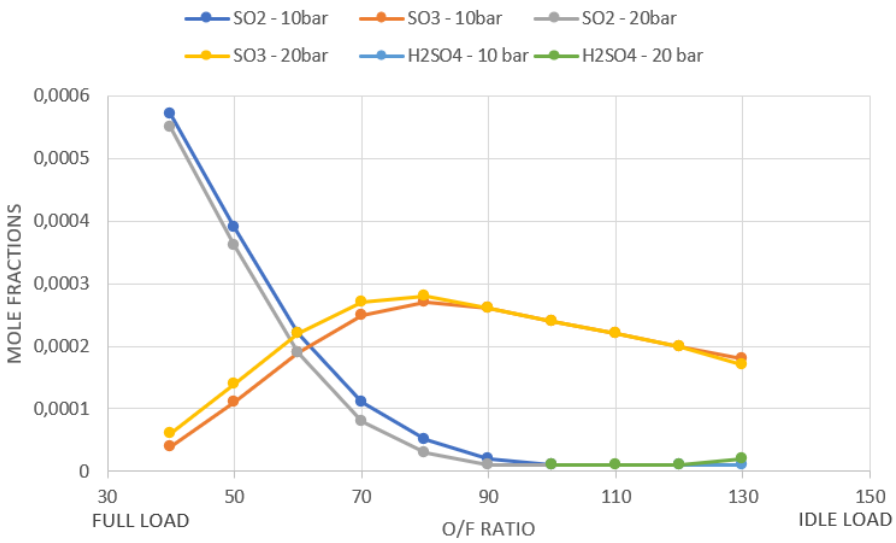

Figure 4.6: Gas Turbine Combustion (CEA).

4.2 Jupyter/ Cantera

Cantera is an open-source chemical kinetics software that can be used to perform calculations for chemical kinetics, thermodynamics, and/or transport processes. This software is suitable for modelling combustion processes and electrochemical processes. Cantera supports multiple interfaces and can be used from Python, C/C+, Fortran and Matlab. In the course of this work, Jupyter/Cantera was used from Python interface to further investigate the influence of temperature on the formation of SO_3. The programme Chemical Equilibrium with Application by NASA used in the previous chapter 4.1 assumes a catalyst

and infinite residence time to calculate the equilibrium. In contrast, Cantera assumes no catalyst and a specific residence time is used for calculation. In reality, during the operation of a gas turbine, there is a certain residence time of the gases.

4.2.1 Code

The entire code can be found in the appendix A and the most important steps are explained below. A gas mixture must be defined by importing an external file that contains necessary thermodynamic property data for further calculation. This is done by adding the following line to the script:

```
gas = ct.Solution('filename.cti')
```

The thermochemistry data was taken from *Glarborg et al.* [68] and *Yilmaz et al.* [69]. As already explained in chapter 6.1, in addition to the composition information, two thermodynamic state functions must be assigned to define a gas mixture:

```
gas.TPX = temperature, pressure, composition
gas.TDX = temperature, density, composition
gas.HPX = specific enthalpy, pressure, composition
gas.UVX = specific internal energy, specific volume, composition
gas.SPX = specific entropy, pressure, composition
gas.SVX = specific entropy, specific volume, composition
```

The state of the gas was modified by adding this line to the script:

```
gas.TPX = T, ct.one_atm, 'SO2:0.04,O2:1,N2:3.74'
```

This line sets the pressure to one atmosphere and specifies the temperature in K as well as the composition in mole.

It is necessary to introduce a reactor, which determines the vessel in which the gas is located as well as the gas flow. For this purpose, an IdealGasConstPressureReactor was defined, which means a homogeneous, constant pressure, zero-dimensional reactor for ideal gas mixtures. Here, the volume of the reactor changes as a function of time to keep the pressure constant. The reactor was introduced by adding the following line to the script:

```
r=ct.IdealGasConstPressureReactor(gas)
```

The simulation must also progress in time. For this, starting time, temperature difference and integrator timesteps must be defined.

```
n_time_steps = 100000
delta_t = 0.01
start_time = 0.0
```

4.2.2 Results

The figure 4.7 shows the mole fractions of SO_2 and SO_3 as a function of time. This plot is the graphical representation of the results of the calculations made using the thermochemical data from *Glarborg et al.* [68]. The calculations made using the thermochemical data from *Yilmaz et al.* [69] led to the same results.

As already described in the literature and with the help of CEA modelling, the SO_3 content increases with decreasing temperatures. In contrast, the SO_2 content decreases with decreasing temperatures. Since Cantera is also a kinetic simulation, it can also be seen that the respective mole fractions react very quickly when the temperature is above the equilibrium temperature.

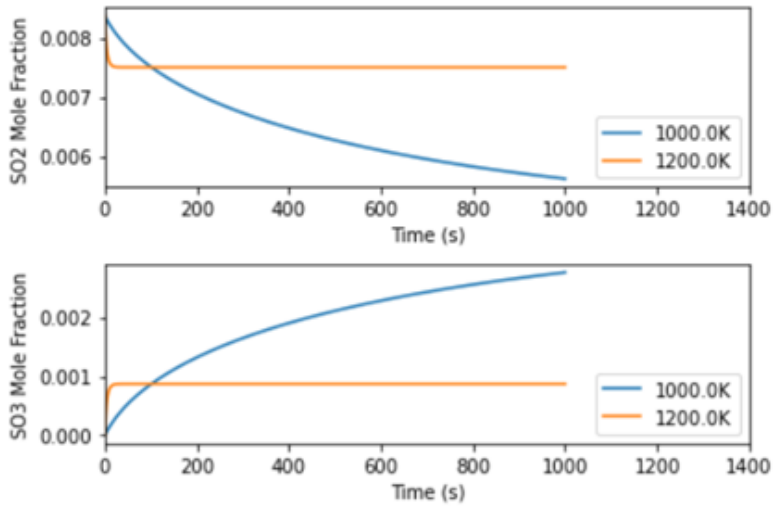

Figure 4.7: Above: Change of SO_2 mole fractions over time
Below: Change of SO_3 mole fractions over time
Calculated with thermodynamic data by *Glarborg et al.* [68].

Chapter 5

Laboratory Work - IPA

Among the wet chemical analysis (chapter 3.2), the Isopropanol Absorption method, in short IPA method, seems promising. In contrast to the CCM method and the salt method, which are also accurate according to the literature, the IPA method does not require the SO_3 to be reacted with moisture to form sulfuric acid but can measure the SO_3 directly. Laboratory tests in the course of this work were carried out at the Vienna University of Technology in the working group of Dr. Helmut Riedl-Tragenreif. The testing rig used for the experiment was set up during a master's thesis project by Dipl.Ing. Oliver E. Hudak and Dipl. Ing. Alexander Scheiber. In this testing rig there is currently no possibility to introduce water, which has two impacts:

- Moisture affects the formation of SO_3 because it shifts the equilibrium (equation 2.9). However, the influence of moisture cannot be experimentally proven at present.
- As there is currently no possibility to introduce water into the testing rig, the IPA method was chosen for the measurement of the SO_3 content.

The following experiments were carried out together with Dipl.Ing. Oliver E. Hudak.

5.1 Testing Rig

The testing rig is made up of 3 system areas, which are explained in more detail in this chapter and can be seen in figure 5.1:

- Upper section where the reaction chamber and 3-zone furnace is located, in which temperatures from 600°C to 950°C can be set.
- Middle section where the gas mixing system is located.
- Bottom section where the wet chemical analysis, i.e. the IPA method for determining the amount of SO_2 and SO_3 and cleaning process takes place.

Since the tubing system must be resistant against corrosive gases such as SO_2 and SO_3, a chemically inert material, namely perfluoro-alkoxy-alkanes (PFA), was selected. It is important that the limiting temperature of 260°C of the piping material is not exceeded. The check valves shown in the figure 5.1 ensure a gas flow in the desired direction.

5.1.1 Gas Mixing Module

In this section of the testing rig, the gases argon, oxygen and SO_2 can be mixed in various ratios. The gases are taken from their respective gas cylinders, with the SO_2 gas cylinder located inside the fume hood for safety reasons. Each gas has its own manual valve to open or close the gas supply. In addition, each gas has a separate mass flow controller (MFC) to set a specific amount of argon, oxygen and SO_2 in standard cubic centimetres per minute (SCCM). GE50A and MKS instruments were used as MFC and JEVATEC Jevaflow FCU-4 was used as control panel, which is connected to the mass flow meters. The maximum values that can be set are 5000 SCCM Ar (carrier and purge gas), 500 SCCM O_2 and 10 SCCM SO_2.

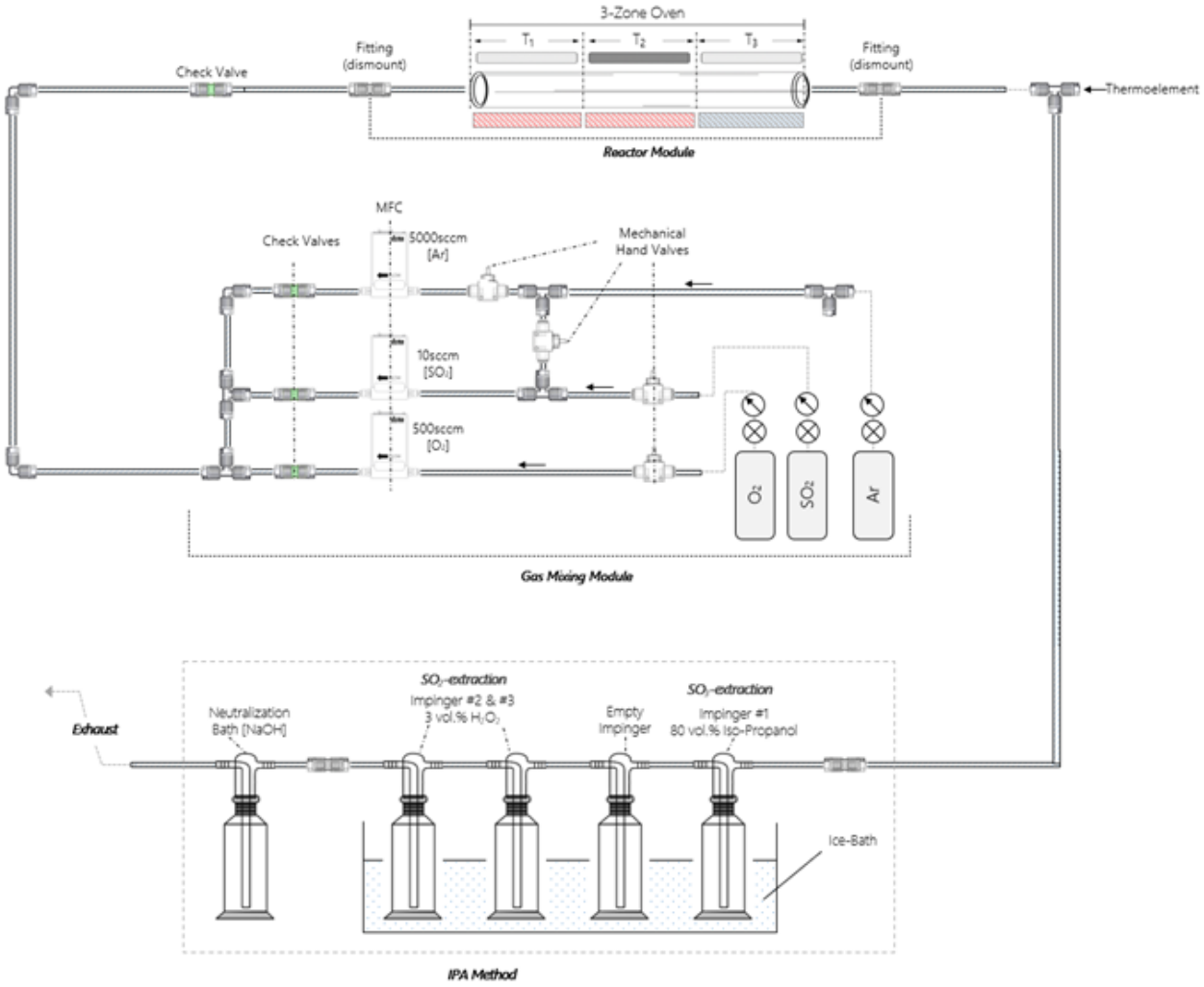

Figure 5.1: set-up of Corrosion Testing Rig to measure SO_2 and SO_3 content, adapted from Dipl.Ing. Oliver E. Hudak.

5.1.2 Reactor Module - Furnace

A horizontal tube furnace is used as reaction chamber in which a temperature range typical for hot corrosion, i.e. 600-950°C, can be set and a constant gas flow is ensured. A quartz glass reactor with an inner diameter of 55mm and a length of 1.1 metres is used for this purpose. In this section, samples can be heated together with a catalyst at a specific temperature. A temperature gradient can be set with a three-zone EZS-3G Carbolite

furnace. It should be noted that at high temperature settings in zone 3, excessively hot gases will escape and enter the PFA pipes, thus exceeding the limiting temperature of the pipes. To protect the pipes from damage, the third zone is used as a cooling zone. The pressure inside the reaction chamber is approximately equal to the ambient pressure, since the quartz glass cannot withstand higher pressures.

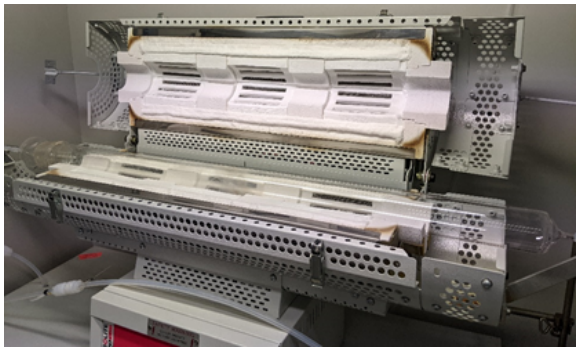

Figure 5.2: Carbolite EZS-3G floating furnace inside the fume hood.

5.1.3 Gas Analysis – IPA Method

As already explained in chapter 3.2.3 IPA Method (experimental setup is depicted in figure 5.1 and 5.3), SO_3 is determined by passing the gas through a solution of 100ml 80% isopropyl alcohol in impinger #1 where the SO_3 is absorbed as sulfate ions. Subsequently by passing the gas through impingers #3 and #4 (each filled with 100ml H_2O_2 solution), the SO_2 content can be determined, where the SO_2 oxidizes to sulfate ions. The resulting sulfate ions can then be measured via titration with barium perchlorate and thorin as an indicator. Since there is no possibility of introducing moisture into this testing rig, there is no need for absorption of sulfuric acid, which is formed by the reaction of SO_3 with water at high temperature in the reaction chamber, in isopropanol. As a result, there is also no need to consider the acid dew point and no risk of liquid sulfuric acid remaining in the piping system. As can be seen in figure 5.3, the method described in the literature [34] was modified by adding an empty impinger between the impinger #1 filled with isopropanol and the two impingers #3 and #4 filled with hydrogen peroxide to improve accuracy and avoid contamination. Finally, a cleaning impinger filled with NaOH is installed to clean the gas from last corrosive residues.

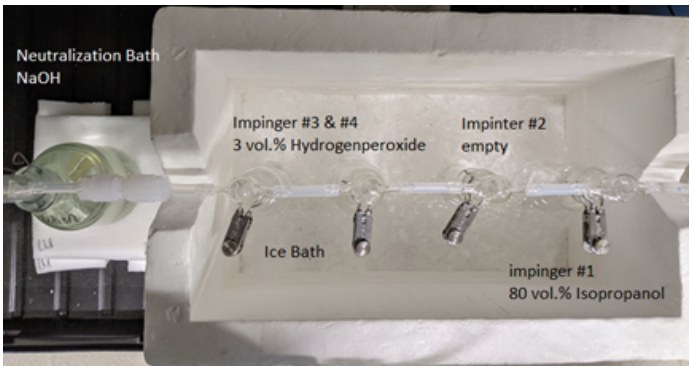

Figure 5.3: Arrangements of the impingers for the IPA Method.

5.2 Procedure of IPA Method

This chapter describes how the contents of the impingers are processed after they have been purged with argon and the SO_3 and SO_2 are captured in the respective impingers.

Table 5.1 shows the equipment and reagents required for the experiment.

Table 5.1: Equipment and Reagents required for the IPA Experiment.

Equipment	Reagents
2x Washbottles (500 ml)	80 vol.% Isopropanol
1x Graduated cylinder (250 ml)	3 vol.% Hydrogenperoxide
1x Graduated cylinder (1000 ml)	Deionized Water
2x Storage bottles (1000 ml)	Ethanol
1x Pipettes (10ml)	Thorin-indicator
1x Pipettes (100 ml)	0.01N Bariumperchlorate
1x Burette (50ml)	
2x Volumetric Flask (250 ml)	
1x Graduated cylinder (100 ml)	

5.2.1 Sample recovery

The contents of Impinger #1, in which all SO_3 should be absorbed, are transferred to a 250ml graduated cylinder. The impinger and the connecting glassware are rinsed with 80vol.% isopropanol. This solution is diluted to 250ml with 80vol.% isopropanol and the contents are stored in a storage-bottle for later analysis. The contents of impinger #3 and

#4, where the 3vol.% H_2O_2 should have absorbed all the SO_2, are transferred to a 1000ml graduated cylinder. The impingers and connecting glassware are rinsed and diluted to 1l with deionized water. The contents are stored in a storage-bottle for later use.

5.2.2 Analytical procedure - Titration

From the storage flask with 250ml content, in which the SO_3 is captured, a 100ml aliquot is transferred to an Erlenmeyer flask for further titration. From the storage flask with 1000ml content, which comes from the impinger #3 and #4, 10ml aliquot is taken and transferred with 40ml isopropanol in an Erlenmeyer flask for further titration. The SO_3 and SO_2 contents are determined separately by the barium-thorin-titration method. The indicator was prepared by dissolving 0.2g Thorin powder in 100ml deionised water. For the titration, 2-4 drops of the indicator Thorin are added to the Erlenmeyer flask and titrated with a 0.01N barium perchlorate solution. The titration was performed at least twice with the respective aliquot of the sample solution. The addition of the $Ba(ClO_4)_2$ precipitates the sulfate contained in the solution as barium sulfate. The addition of the isopropanol is necessary to lower the solubility product of the barium sulfate. It should be titrated from a yellow colour to a red endpoint. The problem that arose here and can be seen in the following figure 5.4 was that the thorin indicator shows more than one colour change. This results in a high standard deviation and a large human error. During developing the method, a specific colour tone was defined to which titration was carried out in order to keep the standard deviation lower. This may not correspond to the real concentration.

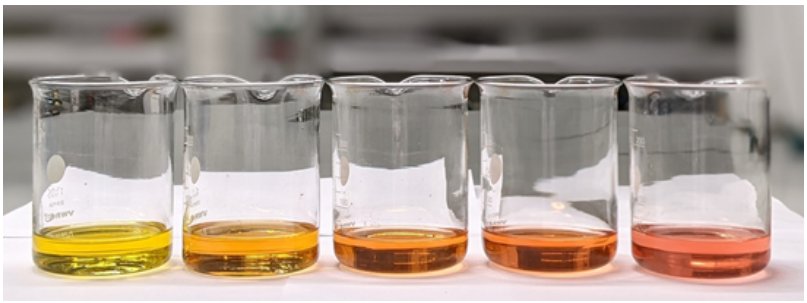

Figure 5.4: Colour change by thorin indicator.

The advantage of titrimetric determination of sulfate ions is that it is a very fast and less tedious method. However, one must expect a low sensitivity since it is very difficult to determine the endpoint exactly with the help of the thorin indicator. An indicator, called Beryl-

lonII or DSNADNS 2-(8-hydroxy-3,6-disulfo-l-naphthylazo)-l,8- dihydroxynaphthalene-3,6-disulfonic acid), could cause a sharper and faster colour change than with Thorin, making the titration more sensitive [70]. Another possibility would be spectrophotometric determination of sulfate ions with a specific amount of excess barium perchlorate and thorin as an indicator. The spectrophotometric wavelength is set to 520nm to determine the excess barium ions [70]. The most accurate method would be ion exchange chromatography, where the sulfate ions are resolved on an anion exchange column and detected by a conductivity detector [71].

5.3 Results

5.3.1 Calibration Experiment

A defined volume flow is passed through the testing rig and the corresponding quantity of SO_2 or SO_3 is absorbed in the respective impingers. In a first experiment only SO_2 gas and argon gas as carrier and purge gas were introduced. There was no oxygen gas supply, hence no SO_3 could be formed by the reaction of SO_2 with O_2. The following input parameters were selected for the experiment: 5 SCCM SO_2. 2000 SCCM Ar; 15 min, Temperature: Zone 1: 500°C, Zone 2: 550°C, Zone 3: 0°C (Zone 3 is not heated in order to protect the PFA tubes connected to the furnace)

The inflowing gas quantity in SCCM can be converted into mol using the calculation shown below. We therefore know the expected concentration and can use this experiment to determine how accurate the measurement is.

$$\dot{m} = \rho_n \cdot \dot{q}$$

Where $\dot{m}$ is the mass flow rate, ρ_n is the density at standard conditions and $\dot{q}$ is the volumetric flow rate.

$$\rho_n = \frac{p_n \cdot M}{Z_n \cdot R_u \cdot T_n}$$

Where p_n is the pressure, M is the molecular weight, Z_n is the fluid compressibility factor, R_u is the universal gas constant and T_n is the temperature.

$$\dot{m}\left[\frac{kg}{s}\right] = \rho_n\left[\frac{kg}{m^3}\right] \cdot \dot{q}\ \left[\frac{cm^3}{min} \cdot \frac{1min}{60s} \cdot \frac{1m^3}{10^6 cm^3}\right]$$

$$\dot{m}\left[\frac{kg}{s}\right] = \frac{p_n\,[Pa] \cdot M\left[\frac{kg}{kmol}\right]}{Z_n R_u\left[\frac{J}{Kkmo}\right] \cdot T_n\,[K]}\ \cdot \dot{q}\ \left[\frac{cm^3}{min} \cdot \frac{1min}{60s} \cdot \frac{1m^3}{10^6 cm^3}\right]$$

Conversion from SCCM to kg/s and vice verca:

$$1\frac{kg}{s} = 6 \cdot 10^7 \cdot \frac{Z_n R_u\left[\frac{J}{Kkmo}\right] \cdot T_n\,[K]}{p_n\,[Pa] \cdot M\left[\frac{kg}{kmol}\right]}\ \cdot SCCM$$

$$1SCCM = 1.6667 \cdot 10^{-8} \cdot \frac{p_n\,[Pa] \cdot M\left[\frac{kg}{kmol}\right]}{Z_n R_u\left[\frac{J}{Kkmo}\right] \cdot T_n\,[K]}\ \cdot \frac{kg}{s}$$

Relationship between SCCM and molar flow rate in kmol/s (assuming ideal gas: $Z_n = 1$) and considering standard conditions:

$$1SCCM = 1.6667 \cdot 10^{-8} \cdot \frac{p_n\,[Pa] \cdot M\left[\frac{kg}{kmol}\right]}{R_u\left[\frac{J}{Kkmo}\right] \cdot T_n\,[K]}\ \cdot \frac{kg}{s}$$

$$1SCCM = 1.6667 \cdot 10^{-8} \cdot \frac{101325\,[Pa] \cdot M\left[\frac{kg}{kmol}\right]}{8314\left[\frac{J}{Kkmo}\right] \cdot 273.15\,[K]}\ \cdot \frac{kg}{s} = 7.436 \cdot 10^{-10} M\left[\frac{kg}{kmol}\right] \cdot \frac{kg}{s}$$

Example for N_2 with molecular weight $M = 2 \cdot 14\frac{kg}{kmol} = 28\frac{kg}{kmol}$

$$1SCCM\,(N_2) = 7.436 \cdot 10^{-10} \cdot 28\frac{kg}{s} = 2.0822 \cdot 10^{-5}\frac{g}{s} = \frac{2.0822 \cdot 10^{-5}\frac{g}{s}}{28\frac{g}{mol}N_2}$$

$$= 7.436 \cdot 10^{-7}\frac{mol}{s} \text{ any gas at } 0°C$$

$$= 6.855 \cdot 10^{-7}\frac{mol}{s} \text{ any gas at } 25°C$$

.

$$\rightarrow \mathbf{1SCCM = 6.855 \cdot 10^{-7}\frac{mol}{s}}$$

Example: 5SCCM SO_2 (for 15Min) in mol:

$$6.855 \cdot 10^{-7} \frac{mol}{s} \cdot 60 \frac{s}{min} \cdot 15min \cdot 5 = \mathbf{0.003085mol} \; - \; \mathbf{desired\ value}$$

$$0.003085mol\ SO_2 \cdot \frac{10ml(aliquot)}{1000ml(total\ volume)} = 0.00003085 \; - \; mol\ to\ titrate$$

$$\frac{0.00003085\ mol\ SO_2}{0.005\ \frac{mol}{L}\ Ba(ClO_4)_2} = \frac{0.00003085\ mol\ SO_2}{0.000005\ \frac{mol}{mL}\ Ba(ClO_4)_2} = 6.17ml\ Ba(ClO_4)_2\ solution - desired\ value$$

Table 5.2 and figure 5.5 show the comparison of the amount of SO_2 expected by the calculation and the amount of SO_2 determined by the titration of 10ml aliquot. As expected, no SO_3 could be detected in the 80vol% isopropanol solution obtained from Impinger #1 because no oxygen gas was added in this experimental setup.

Table 5.2: Comparison of calculated and measured SO_2 values (Calibration Experiment).

Volume $Ba(ClO_4)_2$ [ml]	**SO_2 calculated value [mol]**	**SO_2 measured value [mol]**	**Recovery [%]**
normal set-up with pressure gauge connections right and left.			
2.2	3.08E-05	0.000011	35.66
2.5	3.08E-05	0.0000125	40.52
2.3	3.08E-05	0.0000115	37.28
2.4	3.08E-05	0.000012	38.90
	average value	**0.00001175**	**38.09**
	standard deviation	**5.59E-07**	
Teflon tape was placed around each thread of the fittings to seal them.			
3.3	3.08E-05	0.0000165	53.49
3.6	3.08E-05	0.000018	58.35
2.9	3.08E-05	0.0000145	47.01
	average value	**1.63E-05**	**52.95**
	standard deviaton	**1.43E-06**	

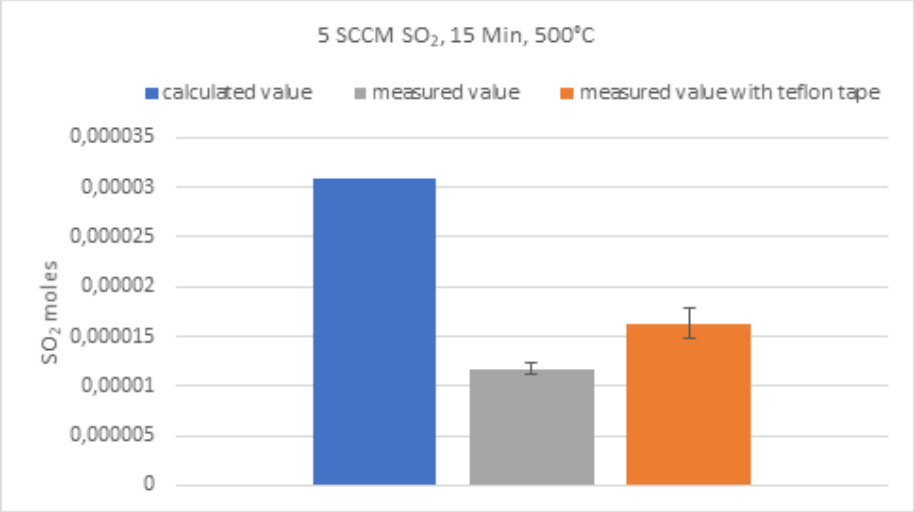

Figure 5.5: Results of the calibration experiment

The result of the calibration experiment shows that the recovery rate is very low and far less SO_2 could be measured than expected. Therefore, a leakage was investigated by mounting wet pH strips on threads and screws. If SO_2 escapes there, it reacts with the water on the pH strip to sulfurous acid (H_2SO_3) and changes the pH value of the indicator paper.

Figure 5.6 shows how the universal indicator paper was clamped in the testing rig and how the colour of the paper changed, indicating an acidic pH value, where the paper was clamped. This indicates that there is a leak and that some of the gas is escaping and cannot be absorbed by isopropanol or hydrogen peroxide.

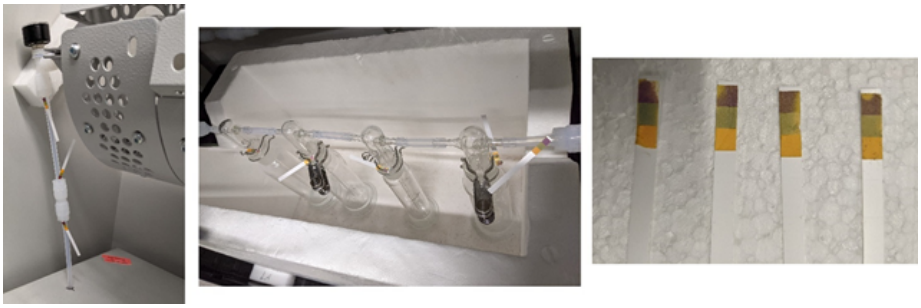

Figure 5.6: Search for a leakage.

Since the recovery rate is very low, one must assume that there is also another reason why so little SO_2 can be determined experimentally. Another reason could be that the gases

do not have enough time to react with isopropanol or H_2O_2 or the contact between the liquids and the gases is too small. One way to improve this would be to put a magnetic stirring bar in each impinger and increase the contact by stirring. Another reason could be that the titration was done only up to a light orange shade, whereas it would be necessary to titrate to the pink endpoint (figure 5.4) Since the transition is very unclear, calibration experiments could be carried out to determine the exact colour of the transition point by, for example, titrating sulphuric acid and then specifying the endpoint using a spectrometer.

5.3.2 SO_3 measurement at 250°C and 450°C

In contrast to the calibration experiments, oxygen gas was also added in the following experiments to allow SO_3 to form. The input parameters were as follows:

- Experiment 1: 1879 SCCM Ar, 500 SCCM O_2, 1 SCCM SO_2
  $\equiv$ 78.95% Ar, 21vol.% O_2, 420vppm SO_2
  Duration: 75min; Temperature: Zone 1: 250°C, Zone 2: 250°C, Zone 3: 0°C
- Experiment 2: 1879 SCCM Ar, 500 SCCM O_2, 1 SCCM SO_2
  $\equiv$ 78.95% Ar, 21vol.% O_2, 420vppm SO_2
  Duration: 75min; Temperature: Zone 1: 450°C, Zone 2: 450°C, Zone 3: 0°C

The SO_2 content obtained from the H_2O_2 solution are tabulated and plotted in figure 5.7 and table 5.3.

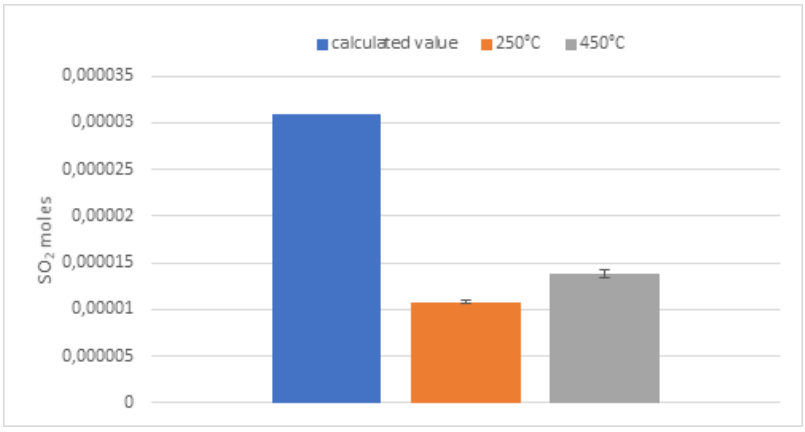

Figure 5.7: SO_2 content for measurement at 250°C and 450°C (78.95vol.% Ar, 21vol.% O_2, 420vppm SO_2).

Table 5.3: Comparison of calculated and measured SO_2 value (measurement at 250°C and 450°C).

Volume $Ba(ClO_4)_2$ [ml]	**SO_2 calculated value [mol]**	**SO_2 measured value [mol]**	**Recovery [%]**
250°C			
2.2	3.08E-05	0.000011	35.66
2.1	3.08E-05	0.0000105	34.04
2.15	3.08E-05	0.00001075	34.85
2.15	3.08E-05	0.00001075	34.85
	average value	**0.00001075**	**34.85**
	standard deviation	**1.77E-07**	
450°C			
2.9	3.08E-05	0.0000145	47.01
2.7	3.08E-05	0.0000135	43.76
2.7	3.08E-05	0.0000135	43.76
2.7	3.08E-05	0.0000135	43.76
	average value	**0.00001375**	**44.57**
	standard deviation	**4.33E-07**	

As already explained in chapter 2.1, the thermodynamic trend [35] says that the SO_2 concentration increases with increasing temperature. The result is consistent with this prediction. Thermodynamically, the SO_3 content should increase with decreasing temperature, but no SO_3 could be detected in this experiment. The reason could be that the kinetics are frozen at low temperatures [36]. The kinetics below 1000K are very slow, which can be seen from modelling results (Figure 4.7). Throughout this chapter, the correlation that as the process temperature increases, the recovery rate increases could be noted, but could not be explained.

This experiment was modelled using Chemical Equilibrium with Application as well as Cantera/Jupyter. Since the modelling using Jupyter also takes time into account, the residence time of the gases in the reaction chamber must be calculated. The calculation is performed as follows:

Residence time calculation for 1 SCCM SO_2, 500 SCCM O_2, 1879 SCCM Ar
Temperature: 250°C/250°C/0°C or 450°C/450°C/0°C

$$\dot{V} = \dot{V}_{Ar} + \dot{V}_{O_2} + \dot{V}_{SO_2} = 2380\ SCCM$$

$$\nu = \frac{4 \cdot \dot{V}}{d^2 \cdot \pi} = \frac{4 \cdot 2380 \frac{cm^3}{min}}{(5.5cm)^2 \cdot \pi} = 100.18 \frac{cm}{min} = 1.0018 \frac{m}{min} = 0.017 \frac{m}{s}$$

$$Residence\ time = \frac{0.4m}{0.017 \frac{m}{s}} = \mathbf{23.53s}$$

The Python code for the modelling can be found in the appendix B. The results obtained from the modelling can be seen in table 5.4:

Table 5.4: Vol.Frac. predicted by Cantera (23.53s) and CEA

	Theory	**Cantera 250°C**	**Cantera 450°C**
SO_2	0.00042017	0.00042017	0.00042017
SO_3	-	2.21E-28	1.15E-14
Total	0.00042017	0.00042017	0.00042017
Recovery		100 %	100 %

	Theory	**CEA 250°C**	**CEA 450°C**
SO_2	0.00042017	1.01E-08	5.52E-07
SO_3	-	0.00042025	0.00042006
Total	0.00042017	0.00042026	0.00042061
Recovery		99.98 %	100.9 %

	Theory	**Lab 250°C**	**Lab 450°C**
SO_2	0.00042017	0.00014642	0.00018729
SO_3	-		
Total	0.00042017	0.00014642	0.00018729
Recovery		34.85 %	44.57 %

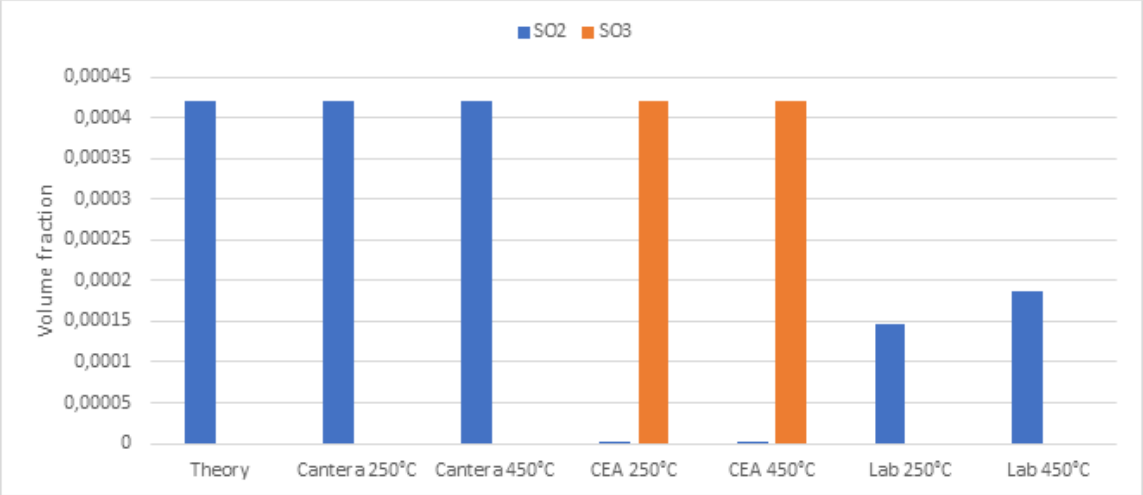

Figure 5.8: Volume Fraction predicted by Cantera (23.53s) and CEA).

The theoretical value is derived from the amount of SO_2 in SCCM into the testing rig, assuming that no SO_3 is produced. Since no catalyst was used in the experiment conducted in the laboratory, the modelling using Cantera reflects the experiment more realistically. In contrast to Cantera, CEA assumes a catalyst and an infinite residence time. Cantera indicates the formation of a SO_3 content, which is not experimentally detectable. Since Cantera also takes kinetics into account, it can be seen that more SO_3 is indeed formed at higher temperatures. By modelling using CEA, it can be seen that the presence of a catalyst converts almost all of the SO_2 to SO_3 and that, as thermodynamics predicts, there is a higher SO_2 content as the temperature increases.

5.3.3 SO_3 measurement at 500°C and 850°C / with and without catalyst

Since no SO_3 could be detected in the measurement experiments at 250°C and 450°C because the kinetics were probably too slow, a higher temperature was selected for the following experiments. In addition, 10 times the initial amount of SO_2 was chosen and it was investigated how the catalyst alumina affects the formation of SO_3. The following parameters were used for the measurement:

- Experiment 1: 1500 SCCM Ar, 500 SCCM O_2, 10 SCCM SO_2
  Duration: 60 min; Temperature: Zone 1: 850°C, Zone 2: 850°C, Zone 3: 0°C
  Without Al_2O_3 catalyst

- Experiment 2: 1500 SCCM Ar, 500 SCCM O_2, 10 SCCM SO_2
  Duration: 60 min; Temperature: Zone 1: 850°C, Zone 2: 850°C, Zone 3: 0°C
  With Al_2O_3 catalyst

- Experiment 3: 1500 SCCM Ar, 500 SCCM O_2, 10 SCCM SO_2
  Duration: 60 min; Temperature: Zone 1: 500°C, Zone 2: 500°C, Zone 3: 0°C
  With Al_2O_3 catalyst

The SO_2 contents determined from these experiments are shown in table 5.5 and diagram 5.9. For titration, a 10ml aliquot was taken and mixed with 40ml of isopropanol before adding 2-4 drops of the thorin indicator.

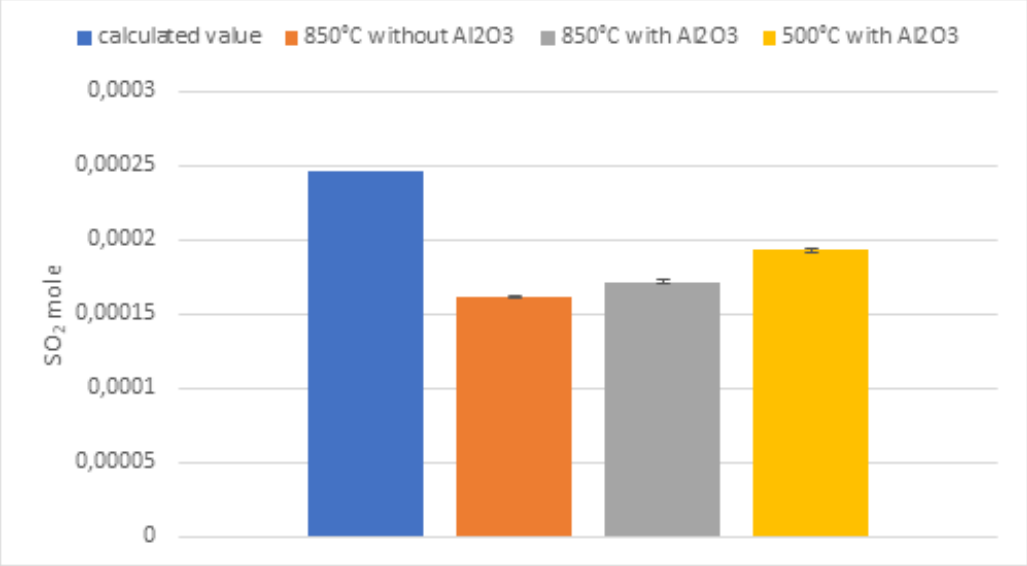

Figure 5.9: SO_2 content for measurement at 850°C & 500°C and with/without catalyst.

Table 5.5: Comparison of calculated and measured SO_2 values (measurement at 850°C and 500°C/ with and without Al_2O_2 catalyst).

Volume $Ba(ClO_4)_2$ [ml]	**SO_2 calculated value [mol]**	**SO_2 measured value [mol]**	**Recovery [%]**
850°C without catalyst Al2O3			
32.2	2.47E-04	1.61E-04	65.24
32	2.47E-04	1.60E-04	64.84
32.3	2.47E-04	1.62E-04	65.44
32.4	2.47E-04	1.62E-04	65.65
32	2.47E-04	1.60E-04	64.84
32.5	2.47E-04	1.63E-04	65.85
32.4	2.47E-04	1.62E-04	65.65
32.5	2.47E-04	1.63E-04	65.85
	average value	**1.61E-04**	**65.42**
	standard deviation	**9.50E-07**	
850°C with catalyst Al2O3			
34.5	2.47E-04	1.73E-04	69.90
34	2.47E-04	1.70E-04	68.89
34.5	2.47E-04	1.73E-04	69.90
34.2	2.47E-04	1.71E-04	69.29
34.6	2.47E-04	1.73E-04	70.10
34.1	2.47E-04	1.71E-04	69.09
34.3	2.47E-04	1.72E-04	69.50
34.4	2.47E-04	1.72E-04	69.70
	average value	**1.72E-04**	**69.55**
	standard deviation	**9.92E-07**	
500°C with catalyst Al2O3			
38.5	2.47E-04	1.93E-04	78.00
38.3	2.47E-04	1.92E-04	77.60
38.8	2.47E-04	1.94E-04	78.61
39	2.47E-04	1.95E-04	79.02
38.6	2.47E-04	1.93E-04	78.21
38.2	2.47E-04	1.91E-04	77.40
38.9	2.47E-04	1.95E-04	78.82
38.4	2.47E-04	1.92E-04	77.80
	average value	**1.93E-04**	**78.18**
	standard deviation	**1.36E-06**	

It may be that SO_3 gas adsorbs on the plastic pipes between the reaction chamber and impinger#1, i.e. adsorbs on macromolecules and diffuses into the PFA material, thus is not able to reach impinger #1. Therefore, the procedure was extended by flushing the pipes

in between and diluting to 250ml with 80 vol.% isopropanol solution in a separate storage flask. This sample was titrated separately. For the determination of SO_3 content, 100ml or 50ml aliquot was taken, mixed with 2-4 drops of thorin indicator and titrated with barium perchlorate. The results can be seen in table 5.6 and 5.10.

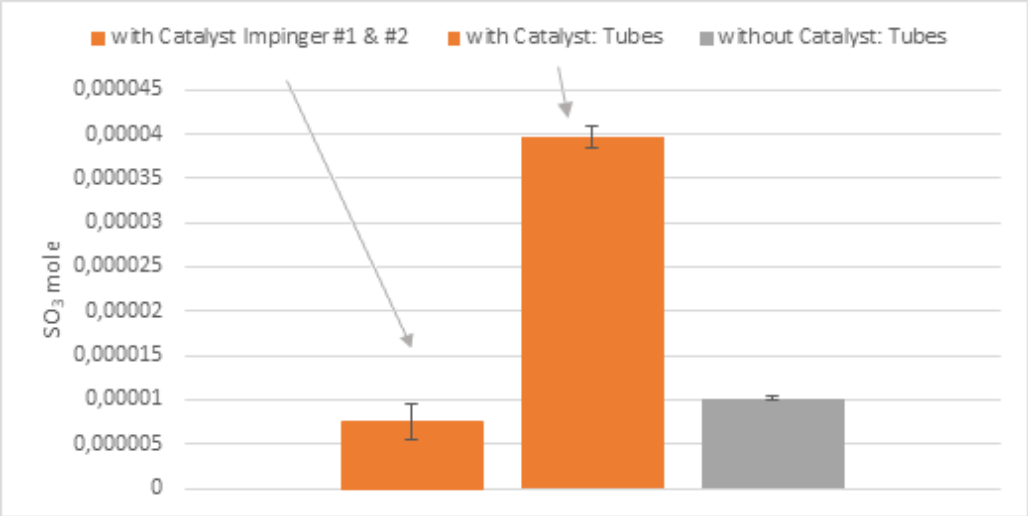

Figure 5.10: SO_3 content for measurement at 850°C with/without catalyst.

Table 5.6: Measured SO_3 value at 850°C with and without catalyst.

Aliquout [ml]	**Volume $Ba(ClO_4)_2$ [ml]**	**SO_3 measured value [mol]**	**Aliquout [ml]**	**Volume $Ba(ClO_4)_2$ [ml]**	**SO_3 measured value [mol]**
850°C - With Al_2O_3 catalyst					
Impinger #1			Pipes between furnace & Impinger #1		
100	1.5	0.0000075	100	8	0.00004
100	2	0.00001	100	8.2	0.000041
50	0.5	0.000005	50	3.8	0.000038
	average value	**0.0000075**		**average value**	**3.9667E-05**
	standard deviation	**2.0412E-06**		**standard deviation**	**1.2472E-06**
850°C - Without Al_2O_3 catalyst					
Impinger #1: no SO_3 detectable			Pipes between furnace & Impinger #1		
			Aliquout [ml]	**Volume $Ba(ClO_4)_2$ [ml]**	**SO_3 measured value [mol]**
			100	2	0.00001
			100	2.1	0.0000105
			50	1	0.00001
				average value	**1.0167E-05**
				standard deviation	**2.357E-07**

Due to the fact that in the presence of Al_2O_3, more SO_3 was formed, it can be assumed that alumina brings the mixture to the thermodynamic equilibrium faster. However, at a reaction temperature of 500°C, no SO_3 was detectable, even though the catalyst Al_2O_3 was present and thermodynamically the formation of SO_3 is favoured at lower temperature. In the presence of the catalyst, more SO_3 was detected in the tubes than in the sample solution taken from impinger #1. Without the catalyst, SO_3 was only detectable in the sample solution originating from the tubes. SO_3 may diffuse into the PFA material, but by using a different plastic material or by coating the inside, the problem could possibly be avoided.

Table 5.7 and figre 5.11 shows the comparison of the theoretically calculated SO_2 volume fraction with the modelling results of Cantera and CEA. For Cantera, the residence time in the furnace had to be calculated (28.57s), as already described in chapter 5.3.2.

Again, the theoretical value corresponds to the SO_2 content, depending on the amount of gas introduced into the testing rig, assuming that no SO_3 is produced. Since CEA assumes a catalyst, the experiment with Al_2O_3 is better represented by CEA and Cantera better mimics the experiment without catalyst.

Table 5.7: Vol.Frac. predicted by Cantera (28.57s) and CEA.

	Theory	**Cantera 850°C**	**CEA 850°C**
SO_2	0.004975	0.004958924	0.00398
SO_3	-	2.02E-05	9.94E-04
Total	0.004975	0.00497917	0.00497759
Recovery		99.92%	99.95%

	Theory	**Lab 850°C with Catalyst**	**Lab 850°C without Catalyst**
SO_2	0.004975	0.00346755	0.003890911
SO_3	-	9.51E-04	2.05E-04
Total	0.004975	0.00441844	0.00409588
Recovery		88.81%	82.33%

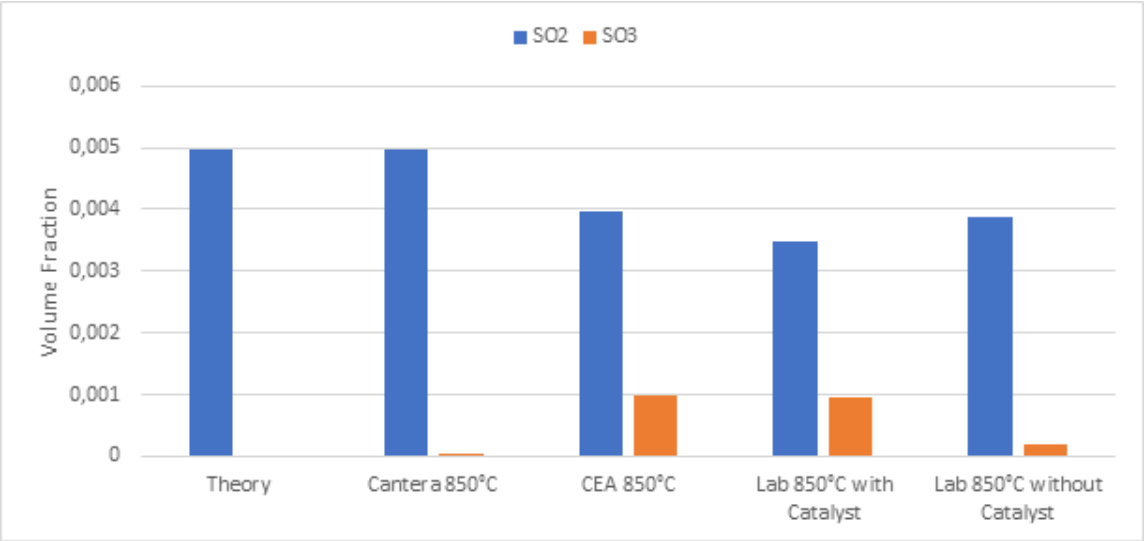

Figure 5.11: Volume Fraction predicted by Cantera (28.57s) and CEA.

Conclusion

Conclusion from the literature review

SO_2 and SO_3 go through jet engines and industrial gas turbines and they corrode turbine blades. It is in the interest of companies like Solar Turbines to minimize the corrosion. However, it is still not really understood how much SO_3 is generated under different conditions.

The following parameters have an influence on the formation of SO_3:

- The formation of SO_3 is thermodynamically preferred when the gas is cooled down. Subsequently, however, the reaction takes place only slowly at low temperatures [34].
- SO_3 in the presence of water is converted to sulfuric acid [28].
- The SO_3 concentration increases with an increasing content of water, O_2, SO_2 and NO [35, 38, 40].
- Platinum catalysts promote the formation of SO_3 [18].
- Some metal oxides contained in the fly ash promote the formation of SO_3, with Fe_2O_3 having the greatest effect [43, 47].
- Alkali- and Alkaline earth metal oxides in the fly ash, such as CaO and MgO capture the SO_3 [42, 50].

The measurement of SO_3 proves to be very difficult due to:

- high reactivity of SO_3,
- presence of many influencing factors (i.e. moisture, temperature) on the SO_2-SO_3 equilibrium,
- formation of sulfuric acid in the presence of water below 500°C [40],
- low SO_3 concentration in comparison to SO_2 concentration and difficult distinction between the gas molecules [34].

Conclusion from the modelling results

The modeling was performed using 2 programs:

- Chemical Equilibrium with Application (CEA) by NASA Lewis Research Center: assumes a catalyst, does not consider kinetics, infinite residence time.
- Cantera used from Python: no catalyst, considers kinetics, well defined residence time. The thermochemical data for the Cantera modelling were taken from *Glarborg et al.* [68] and *Yilmaz et al.* [69].

Modelling using CEA provided some very helpful predictions:

- Below 700°C SO_3 is predominant species, and above 700°C SO_2 is predominant.
- In the presence of moisture the temperature should be kept above 400°C to prevent the rapidly progressing corrosion caused by sulfuric acid and especially above 200°C to prevent liquid sulfuric acid to form drops and films on the material.
- CO_2 has no influence on the formation of SO_3.
- The SO_3 concentration increases with increasing content of SO_2.

In the simulation by Cantera, the mole fractions of SO_2 and SO_3 could be plotted as a function of time and it could be seen that the reaction rate of SO_2 depends on temperature. The SO_2 content decreases with decreasing temperatures and decreases very quickly when the temperature is above the equilibrium temperature.

Conclusion of experimental measurement of SO_3 via IPA Method

Among the wet chemical analyses, only the controlled condensation method, the salt method and the isopropanol absorption method seem promising. Due to the given resources the IPA Method was chosen, because this method allows direct determination of SO_3 without having to first convert it to H_2SO_4. A very well-defined amount of gas is passed through a corrosion testing rig where a well-defined temperature can be set and, if necessary, a catalyst can be added before it reaches the analytical method. The SO_3 content can be determined via IPA Method by passing the gas through a solution of 80% isopropanol, where the SO_3 is absorbed as sulfate ions. Simultaneously, the SO_2 content can be determined by passing the gas through two impingers filled with 3vol.% H_2O_2 solution, where the SO_2 oxidizes to sulfate ions. The resulting sulfate ions can then be measured via titration with barium perchlorate and thorin as an indicator. To prevent contamination, the method was modified by placing an empty impinger between the impinger filled with isopropanol to absorb SO_3 and the two impingers filled with hydrogen peroxide to absorb SO_2 . Since the indicator thorin does not show a sharp colour change, it is difficult to determine an exact endpoint. Spectrophotometric determination of sulfate ions or ion exchange chromatography with a conductivity detector would be more sensitive methods, but they do not allow such a rapid and simple determination of sulfate ions as titrimetric determination does. When comparing the laboratory results with the theoretical value, a low recovery rate can be observed. This could have several reasons:

- A gas leak
- The titration was not carried out to the pink endpoint but stopped at a lighter shade of orange.
- The contact between the gases (SO_2 and SO_3) and the absorbing liquids ($(CH_3)_2CHOH$ and H_2O_2) was too short or too small. A magnetic stirrer in the impinger could counteract this effect a little.

In contrast to the experimental results, the modelling results provide good indications in terms of the effect of temperature and moisture. For future work, it would be useful to allow moisture to be added into the corrosion testing rig and thus possibly test other wet chemical analysis methods and determine the effect of the moisture experimentally. Another feature

that could also be very useful would be pipes made of another inert material that allows the limiting temperature of 260°C to be exceeded.

Nevertheless, laboratory experiments can mirror the real situation and it could be shown that alumina acts as a catalyst and brings the mixture to the thermodynamic equilibrium faster. According to literature laboratory experiments indicate, that platinum catalysts promote the formation of SO_3, thus the corrosion of nickel is accelerated as well, but to date there is no literature comparing different catalysts (Fe_2O_3, Al_2O_3, TiO_2, etc.). The effect of different catalysts on the formation of SO_3 could be tested by placing different catalysts in the reaction chamber, while other conditions remain constant.

Given the fact that the corrosive effect of SO_3 is known, there is not enough literature about the parameters influencing SO_3 formation and there is no sufficiently accurate measurement method. With some improvements, wet chemical analysis techniques could be used systematically to assess the effect of different catalysts and different levels of moisture to create a model. This model could then be verified on gas turbines and would be suitable for predicting the corrosion load. The above-mentioned information might be useful in determining the location of the engine installation, if a rough estimation of the environmental influences and sulphur-content in the fuel is known. The final vision is to connect the engines to a detector, so that the SO_3 content can be measured continuously during operation.

Appendix

Appendix A: Effect of Temperature

```
import sys
import numpy as np
import cantera as ct
import matplotlib.pyplot as plt
```

```
#gas = ct.Solution('SO2_SO3_Gaseous_alkali.cti')
gas = ct.Solution('SO2_SO3_thermal_dissociation.cti')
```

```
Temperature_list = np.linspace(1000, 1200, num=2, endpoint=True)
```

```
fullData = []
n_time_steps = 100000
delta_t = 0.01
start_time = 0.0
```

```
for T in Temperature_list:
    print (T)
    gas.TPX = T, ct.one_atm, 'SO2: 0.04, O2:1, N2: 3.74'
    r=ct.IdealGasConstPressureReactor(gas)
    #r=ct.IdealGasReactor(gas)
    sim = ct.ReactorNet([r])
    time = start_time
    times = np.zeros(n_time_steps)
    data = np.zeros((n_time_steps,3))

    print('%10s %10s %14s %14s %14s' % ('t [s]','T [K]','P [Pa]','X_SO2','X_SO3'))
    for n in range(n_time_steps):
        time += delta_t
        sim.advance(time)
        times[n] = time # time in s
        data[n,0] = r.T
        data[n,1:] = r.thermo['SO2','SO3'].X
        print('%10.3e %10.3f %14.6f %14.6e %14.6e' % (sim.time, r.T, r.thermo.P,
              r.thermo['SO2'].X, r.thermo['SO3'].X))
    fullData.append(data)
```

.

Appendix B: Modelling of Lab Work

```
import sys
import numpy as np
import cantera as ct
import matplotlib.pyplot as plt
```

```
from IPython.display import set_matplotlib_formats
set_matplotlib_formats('pdf', 'png')
plt.rcParams['savefig.dpi'] = 75
#plt.rcParams['figure.autolayout'] = False
plt.rcParams['figure.figsize'] = 10, 6 # width, height
plt.rcParams['axes.labelsize'] = 20
plt.rcParams['axes.titlesize'] = 20
plt.rcParams['font.size'] = 20
plt.rcParams['lines.linewidth'] = 4.0
plt.rcParams['lines.markersize'] = 8
plt.rcParams['legend.fontsize'] = 20
#plt.rcParams['text.usetex'] = True
plt.rcParams['font.family'] = "serif"
```

```
gas = ct.Solution('SO2_SO3_Gaseous_alkali.cti')
#gas = ct.Solution('SO2_SO3_thermal_dissociation')
```

```
fullData = []
n_time_steps = 300
delta_t = 0.1
start_time = 0.0
```

```
    gas.TPY = 250, ct.one_atm, 'SO2:10, O2:500, Ar:1500'
    r=ct.IdealGasConstPressureReactor(gas)
    #r=ct.IdealGasReactor(gas)
    sim = ct.ReactorNet([r])
    time = start_time
    times = np.zeros(n_time_steps)
    data = np.zeros((n_time_steps,3))

    print('%10s %10s %14s %14s %14s' % ('t [s]','T [K]','P [Pa]','Y_SO2','Y_SO3'))
    for n in range(n_time_steps):
        time += delta_t
        sim.advance(time)
        times[n] = time # time in s
        data[n,0] = r.T
        data[n,1:] = r.thermo['SO2','SO3'].Y
        print('%10.3e %10.3f %14.6f %14.6e %14.6e' % (sim.time, r.T, r.thermo.P,
                r.thermo['SO2'].Y, r.thermo['SO3'].Y))
    fullData.append(data)
```

.

List of Figures

List of Tables

Bibliography

[1] C. Lechner and J. Seume, *"Stationäre Gasturbinen"*. Springer Berlin Heidelberg,Springer Vieweg, 2019.

[2] R. K. B. Brun, *"Introduction to Gas Turbine Theory"*. 2019.

[3] A. Nasiri, F. Bayat, S. Mobayen and H. Hosseinnia, *"Gas Turbine Power Regulation Subject to Actuator Constraints, Disturbance and Measurement Noises"*. 2021.

[4] R. Burgel, H. J. Maier and T. Niendorf, *"Handbuch Hochtemperatur-Werkstofftechnik - Grundlagen Werkstoffb"*. 2011.

[5] N. Eliaz, G. Shemesh and R. M. Latanision, *"Hot corrosion in gas turbine components"*. 2002.

[6] T. M. Pollock and S. Tin, *"Nickel-based superalloys for advanced turbine engines: Chemistry, microstructure, and properties"*. Journal of Propulsion and Power, 2006.

[7] L. Rolls-Royce, *"The jet engine, vol. 5th edition"*. Rolls-Royce, 1996.

[8] R. C. Reed, *"The superalloys: fundamentals and applications"*. Cambridge University Press, 2006.

[9] H. T. Kim, S. S. Chun, X. X. Yao, Y. Fang and J. Choi, *"Gamma prime precipitating and ageing behaviours in two newly developed nickel-base superalloys"*. 1997.

[10] Rösler, J., Näth, O., Jäger, S. et al., *"Nanoporous Ni-based superalloy membranes by selective phase dissolution."*. Technical University Braunschweig, March 2005.

[11] Y. M. Eggeler, *"Nano- and Microstructural Evolution"*. PhD Thesis, Erlangen-Nürnberg, 2018.

[12] E. Kunze, *"Korrosion und Korrosionsschutz"*. Germany: Wiley-VCH, 2001.

[13] W. Gao and Z. Li, *"High Temperature Corrosion"*. Developments in High Temperature Corrosion and Protection of Materials, 2008.

[14] G. W. Meetham and M. H. van de Voorde, *"Materials for High Temperature Engineering Applications"*. Springer Berlin Heidelberg, 2000.

[15] A. Demirbas, *"Sulfur removal from crude oil using supercritical water"*. Petroleum Science and Technology,2016.

[16] T. Pecoraro and R. Chianelli, *"Hydrodesulfurization Catalysis by Transition Metal Sulfides"*. Journal of Catalysis 67, 430-445, 1981.

[17] S. Mrowec, *"The Problem of Sulfur in High-Temperature Corrosion"*. 1995.

[18] Kofstad, *"High Temperature corrosion"*.

[19] C. Xu and W. Gao, *"Pilling-Bedworth ratio for oxidation of alloys"*. Springer Verlag, 2000.

[20] R. V. McVay, P. Williams, G. H. Meier and F. S. Pettit, *"Oxidation of Low Sulfur Single Crystal Nickel-Base Superalloys"*. 2012.

[21] M. DeCrescente and N. Bornstein, *"Formation and Reactivity Thermodynamics of Sodium Sulfate with Gas Turbine Alloys"*. Corrosion vol. 24, no. 5 , 1968.

[22] D. Rezakhani, *"MSc Thesis"*. Shiraz University, 1998.

[23] F. Pettit and G. Meier, *"Oxidation and Hot Corrosion of Superalloys"*. Superalloys, 1984.

[24] J. Nicholls and N. Simms, *"Basic Concepts, High Temperature Corrosion"*. Shreir's Corrosion, Cranfield University, Bedfordshire, 2010.

[25] N. Birks , G. Meier and F. Pettit, *"Introduction to High Temperature Oxidation of Metals"*. Cambridge University Press, Cambridge, 2006.

[26] M. Joyce, X. Wu and P. Read, *"The effect of environmental and orientation on fatigue crack growth behaviour of CMSX-4 nickel base single crystal at 650°C"*. Materials Letters, 2004.

[27] K. Luthra, *"Low temperature hot corrosion of cobald-base alloys: part II. Reaction Mechanism"*. Metallurgical Transaction A, October 1982.

[28] D. Fleig, F. Normann, K. Andersson, F. Johnsson and B. Leckner, *"The fate of sulphur during oxy-fuel combustion of lignite"*. Energy Procedia, 2009.

[29] C. F. Cullis und M. F. R. Mulcahy, *"The Kinetics of Combustion of Gaseous Sulphur Compounds"*. 1972.

[30] T. Gheno and B. Gleeson, *"On the Hot Corrosion of Nickel at 700 °C"*. Oxidation of Metals, 2015.

[31] L. Hindiyarti, P. Glarborg and P. Marshall, *"Reactions of so3 with the O/H radical pool under combustion conditions"* Journal of Physical Chemistry A, 2007.

[32] R. Hardman and R. Stacy, *"Estimating Sulfuric Acid Aerosol Emissions from Coal-Fired Power Plants"*. 1998.

[33] EPRI, C. Dene and R. Himes, *"Continuous Measurement Technologies for SO 3 and H 2 SO 4 in Coal-Fired Power Plants"*. 2004.

[34] D. Fleig, E. Vainio, K. Andersson, A. Brink, F. Johnsson and M. Hupa, *"Evaluation of SO 3 measurement techniques in air and oxy-fuel combustion"*. Energy and Fuels, 2012.

[35] L. Duan, Y. Duan, Y. Sarbassov, Y. Li and E. J. Anthony, *"SO3 formation under oxy-CFB combustion conditions"*. International Journal of Greenhouse Gas Control, 2015.

[36] Y. Sarbassov, L. Duan, V. Manovic and E. J. Anthnoy, *"Sulfur trioxide formation/emissions in coal-fired air- and oxy-fuel combustion processes: a review"*. Society of Chemical Industry and John Wiley and Sons, Ltd., Bedford, Bedfordshire, UK, 2018.

[37] D. Fleig, *"Experimental and Modeling Studies of Sulfur-Based Reactions in Oxy-Fuel Combustion"*. Universität Kassel, Göteburg, Sweden, 2012.

[38] D. Fleig, K. Andersson, F. Normann and F. Johnsson, *"SO3 Formation under oxyfuel combustion conditions"*. Industrial and Engineering Chemistry Research, 2011.

[39] D. Fleig, K. Andersson and F. Johnsson, *"Influence of operating conditions on SO3 formation during air and oxy-fuel combustion"*. Industrial and Engineering Chemistry Research, 2012.

[40] A. Andersen, P. Kofstad and P. K. Lillerud, *"High Temperature Corrosion of Nickel and Dilute Nickel-based Alloys in (S0z-02)/S03 Mixtures"*. 1987.

[41] L. Brachert, T. Kochenburger and K. Schaber, *"Facing the sulfuric acid aerosol problem in flue gas cleaning Pilot plant experiments and simulation"*. Aerosol Science and Technology, 2013.

[42] R. Spörl et al., *"SO3 emissions and removal by ash in coal-fired oxy-fuel combustion"*. Energy and Fuels, 2014.

[43] L. P. Belo et al., *"High-temperature conversion of SO2 to SO3: Homogeneous experiments and catalytic effect of fly ash from air and oxy-fuel firing"*. Energy and Fuels, 2014

[44] E. Vainio, D. Fleig, A. Brink, K. Andersson, F. Johnsson and M. Hupa, *"Experimental evaluation and field application of a salt method for SO3 measurement in flue gases"*. Energy and Fuels, 2013.

[45] J. O. L. Wendt and C. Sternling, *"Catalysis of S02 Oxidation by Nitrogen Oxides"*. 1973.

[46] *"Sulfur trioxide measurement technique for SCR units"*. Danish Environmental Protection Agency, 2016.

[47] J. P. Dunn, P. R. Koppula, H. G. Stenger and I. E. Wachs *"Oxidation of sulfur dioxide to sulfur trioxide over supported vanadia catalysts"*. 1998.

[48] J. Svachula et al., *"Oxidation of SO2 to SO3 over Honeycomb DeNoxing Catalysts"*. 1993.

[49] S. C. Alexander Fateev, *"Sulfur trioxide measurement technique for SCR units"*. Danish Environmental Protection Agency, 2016.

[50] P. Marier and P. Dibbst, *"THE CATALYTIC CONVERSION OF SO2 TO SO, BY FLY ASH AND THE CAPTURE OF SO2 AND SO3 BY C-a0 AND Mg0"*. 1971.

[51] A. Krueger, K. Yang and N. Krotkov, *"Enhanced monitoring of sulfur dioxide sources with hyperspectral UV sensors, vol. 7475"*. Remote Sensing of Clouds and the Atmosphere XIV, 2009.

[52] A. Krueger, N. Krotkov and S. Carn, *"El Chichon: The genesis of volcanic sulfur dioxide monitoring from space"*. Journal of Volcanology and Geothermal Research, vol. 175, no. 4, 2008.

[53] NASA, *"SO2 climatology from satellite instruments"*.

[54] ESA, *"sentinel-5 precursor"*. 2013.

[55] R. F. Maddalone, S. F. Newton, R. G. Rhudy and R. M. Statnick, *"Laboratory and Field Evaluation of the Controlled Condensation System for SO3 Measurements in Flue Gas Streams"*. Journal of the Air Pollution Control Association, vol. 29, no. 6, 1979.

[56] Y. Li et al., *"Experimental method for observing the fate of SO3/H2SO4 in a temperature-decreasing flue gas flow: Creation of state diagram, Fuel, vol. 249"*. 2019.

[57] F. Kelman, *"Direct method on determination of the sulfuric acid in solution"*. Zavod Lab, 1952.

[58] R. J. Jaworowski and S. S. Mack, *"Evaluation of Methods for Measurement of SO3/H2SO4 in Flue Gas"*. Journal of the Air Pollution Control Association, vol. 29, no. 1, 1979.

[59] ncasi, *"Method 8A-Determination of sulfuric acid vapor or mist and sulfur dioxide emissions from kraft recovery furnaces"*. 1996.

[60] B. Dellinger, G. Grotecloss, C. R. Fortune, J. L. Cheney and J. B. Homolya, *"Committee on Biological Effects of Atmospheric Pollutants, Division of Medical Sciences"*. 1963.

[61] K. P. Furlan, C. Binder, A. N. Klein and J. D. B. de Mello, *"Thermal Stability of the MoS2 Phase in Injection Moulded 17-4 PH Stainless Steel"*. Journal of Materials Research and Technology, vol. 1, no. 3, 2012.

[62] D. D. Stuart, *"Acid dewpoint temperature measurement and its use in estimating sulfur trioxide concentration"*. 2010.

[63] P. Jackson, D. Hilton and J. Buddery, *"Continuous measurement of sulphuric acid vapour in combustion gases using a portable automatic monitor"*. J Inst Energy, 1981.

[64] Y.-H. Kiang, *"Predicting Dew Points Of Acid Gases"*. 2017.

[65] J. G. Ibanez, C. F. Batten and W. E. Wentworth, *"Simultaneous determination of SO3(g) and SO2(g) in a flowing gas"*. Industrial and Engineering Chemistry Research, vol. 47, no. 7, 2008.

[66] Gordon Sanford and B. J. McBride, *"Computer Program for Calculation of Complex Chemical Equilibrium Compositions and Applications"*. Cleveland, Ohio: NASA, 1994.

[67] R.-R. p. 1986, *"The Jet engine"*. 2015. Fifth edition Hrsg., Derby, England, 1996, pp. 41- 43.

[68] P. Glarborg und P. Marshall, *"Mechanism and modeling of the formation of gaseous alkali sulfates"*. Denmark: Combustion and Flame, 2004.

[69] A. Yilmaz, L. HIndiyarti, A. D. Jensen, P. Glarborg and P. Marshall, *"Thermal Dissociation of SO3 at 1000 - 1400 K"*. The Journal of Physical Chemistry , June 2006.

[70] H.Hoon, *"Microdetermination of sulfate in environmental samples"*. Thesis, Texas Tech University, 1983.

[71] T. S. S. a. W. C. B. Hamish. Small, *"Novel ion exchange chromatographic method using conductimetric detection"*. Analytical Chemistry, 1975.

[72] William J. Mitchell, M.Rodney Midgett, Jack C. Suggs, *"Precision estimates for epa test method 8—SO2 and H2SO4 emissions from sulfuric acid plants"*. Atmospheric Environment, 1967. Volume 13, Issue 1, Pages 179-182.

[73] A. K. Singh, N. Louat and K. Sadananda, *"Dislocation network formation and coherency loss around gamma- prime precipitates in a nickel- base superalloy"*.